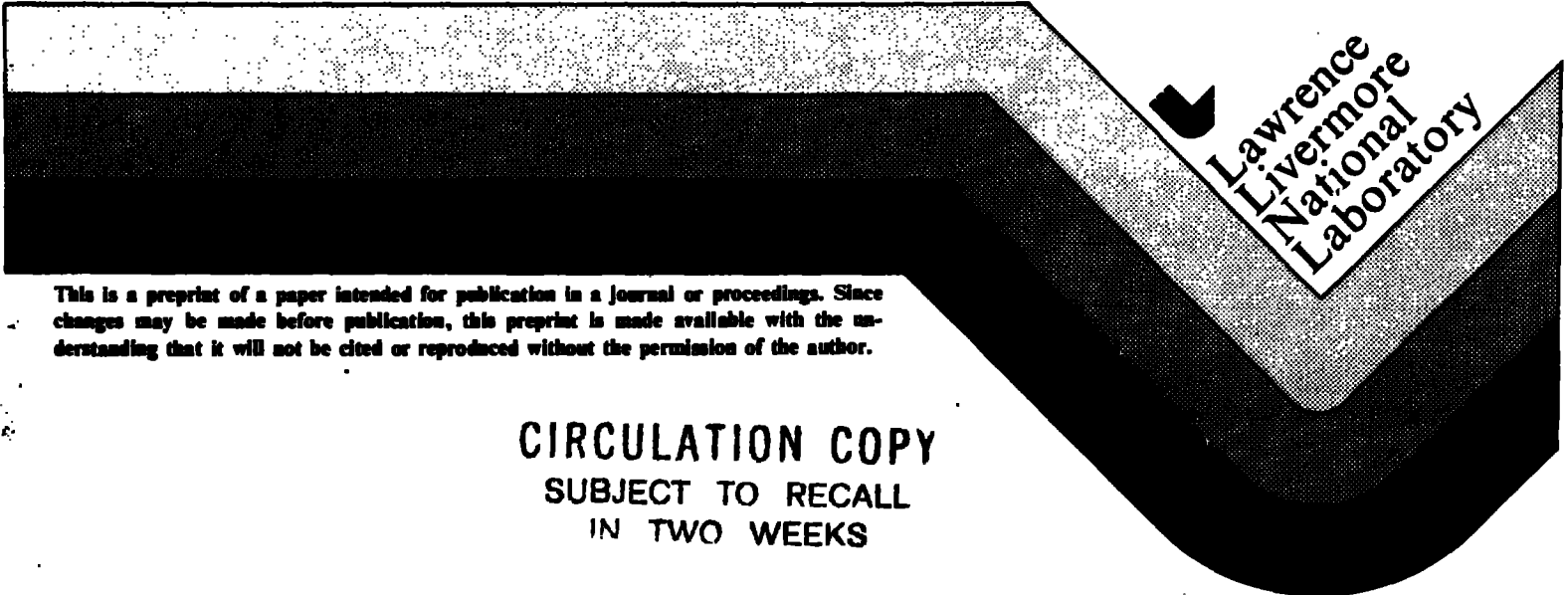# STRUCTURE-PROPERTY RELATIONS
OF EPOXIES USED AS COMPOSITE MATRICES

Roger J. Morgan

BOOK CHAPTER
ADVANCES IN POLYMER SCIENCES
"EPOXY RESINS AND COMPOSITES"

January 25, 1985

CIRCULATION COPY
SUBJECT TO RECALL
IN TWO WEEKS

Lawrence Livermore National Laboratory

DISCLAIMER

STRUCTURE-PROPERTY RELATIONS OF EPOXIES USED AS COMPOSITE MATRICES*

R. J. Morgan

Lawrence Livermore National Laboratory, L-338
University of California, P. O. Box 808
Livermore, California, U.S.A. 94550

The structure-deformation/failure process-mechanical property relations of epoxies used as matrices in high performance fibrous composites are presented. Such composites are fabricated either from carbon fiber-epoxy prepregs or by filament winding. The parameters that affect the processing, cure reactions and the resultant chemical and physical structure of the epoxies are discussed. The deformation and failure processes of these glasses are described. The structural parameters that control the deformation and failure processes, the mechanical response and aging of epoxies are addressed and means of improving their processing and performance are described.

A. INTRODUCTION

The increasing use of high-performance, fibrous composites in critical structural applications has led to a need to predict the lifetimes of these materials in service environments. To predict the durability of a composite in service environment requires a basic understanding of (1) the microscopic deformation and failure processes of the composite; (2) the significance of the fiber, epoxy matrix and fiber-matrix interfacial region in composite performance; and (3) the relations between the structure, deformation and failure processes and mechanical response of the fiber, epoxy matrix and their interface and how such relations are modified by environmental factors.

In this paper we review our studies on the structure-property relations of epoxy matrices used in high-performance fibrous composites that are fabricated either from C fiber-epoxy prepregs or by filament winding. We consider the parameters that affect the processing, cure reactions and resultant chemical and physical structure of these crosslinked glasses. The structural parameters that control the deformation and failure modes, mechanical response and service environment aging of these epoxies are addressed. We, also, discuss epoxy systems that exhibit superior processing, thermal and mechanical properties relative to those presently utilized as composite matrices.

B. PROCESSING AND CHEMICAL STRUCTURE OF EPOXIES USED IN FILAMENT WOUND COMPOSITES

B.I. INTRODUCTION

Epoxy resins utilized in forming filament-wound composites must possess low viscosities (η's) and long gel-times at 23°C. To minimize unreacted starting materials in the finally cured composite requires the chemical cure reactions of the epoxy system must be simple. Furthermore, the number of chemical starting components in the resin must be small to minimize mixing problems that would result in variable thermal and mechanical properties. The toxicity of the resin chemical starting materials must be low. Also, the epoxy system must attain full cure at relatively low post-cure temperatures, <150°C, to minimize the development of fabrication strains in the composite.

Amine-cured diglycidyl ether of bisphenol-A (DGEBA) epoxies are the principal matrices used in filament wound composites. Pure DGEBA, DER332 (Dow)** epoxide cured with an aliphatic polyethertriamine, Jeffamine T403 (Jefferson) is a commonly used epoxy for filament wound Kevlar 49 composites. The chemical structures of the amine and epoxide monomers are shown in Fig. 1. We have studied the structure-property relations of the DGEBA-T403 epoxy in some detail.[1]

**Reference to a company or product name does not imply approval or recommendation of the product by the University of California or the U.S. Department of Energy to the exclusion of others that may be suitable.

B.II. CURE REACTIONS

The amine-cured DGEBA epoxies utilized as matrices for filament wound composites generally form exclusively from epoxide-amine addition reactions (1).

$$R_1CH\text{-}CH_2 + R_2NH_2 \rightarrow R_1CH(OH)CH_2NHR_2 \tag{1}$$
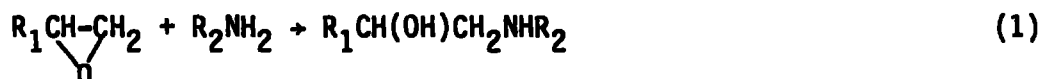
The nature of the cure reactions in these epoxies can be confirmed by monitoring the epoxide consumption via near infra-red spectroscopy for a series of epoxide-amine mixtures containing a range of amine contents. A plot of % epoxide consumption vs. amine concentration for DGEBA-T403 epoxies is illustrated in Fig. 2. This plot confirms that the DGEBA-T403 epoxy system forms exclusively from epoxide-amine addition reactions, because (i) 100% epoxide consumption is attained at the stoichiometric amine concentration associated with exclusive epoxide-amine addition cure reactions and (ii) extrapolation of this plot to zero amine content indicates there is no epoxide consumption i.e. there are no epoxide homopolymerization reactions.

Characterization of the epoxy cure reactions ensures that a composite can be fabricated and the epoxy is fully cured, assuming that the epoxide and amine starting components are initially homogeneously mixed.

B.III. IMPROVED FILAMENT WINDING EPOXIES

The toughness and mechanical performance of a filament wound composite component is enhanced by crack deflection mechanisms and/or molecular flow occurring in the epoxy matrix. The inhibition of crack propagation through a bundle of fibers in a composite can occur by deflection of the crack parallel to the fiber axis by either propagation along the fiber matrix interface and/or through the fiber itself. A poor fiber-matrix interfacial bond and/or microscopic fiber failure by splitting will both enhance these crack deflection toughening mechanisms. The composite performance can also be enhanced under load by molecular flow occurring in the epoxy matrix. Molecular flow is enhanced as T_g is approached because the glassy-state free volume is increased. However, the epoxy matrix cannot be too soft otherwise the composite will readily buckle in compression. In the case of filament-wound Kevlar 49-epoxy composites the poor fiber-interfacial strength, the microscopic splitting of the fibers and matrix ductility all enhance composite mechanical performance.[2,3] However, for C fiber-epoxy filament wound composites the fiber-matrix interface is generally stronger than for Kevlar 49 composites and the C fiber fails without longitudinal fiber splitting. Hence, for C-fiber epoxy composites the matrix is the principal component that affects composite toughness, and this matrix must be tough through a wide temperature range and possess a $T_g > 120°C$. This requires that epoxy matrices for filament-wound C-fiber structures are (i) processible at 23°C, (ii) fully reacted upon post-curing <150°C, (iii) simple chemical and physical systems with limited toxicity and (iv) tough from 23-125°C.

To attain the requirements of an epoxy matrix utilized in filament-wound C fiber-epoxy composites we have considered the characteristics required of the amine curing agent molecule. To ensure long gel times at 23°C requires that the primary amine-epoxide (P.A.-E) reaction rate is considerably greater than the rate of the secondary amine-epoxide (S.A.-E) reaction, and that the S.A. reaction does not occur at low temperatures. Furthermore, to attain low 23°C η's and low post-cure temperatures (to achieve full cure) the amine molecule must be relatively flexible. It was determined that 2,5 dimethyl 2,5 hexane diamine (DMHDA),

$$H_2N-\overset{\overset{\displaystyle CH_3}{|}}{\underset{\underset{\displaystyle CH_3}{|}}{C}}-CH_2-CH_2-\overset{\overset{\displaystyle CH_3}{|}}{\underset{\underset{\displaystyle CH_3}{|}}{C}}-NH_2$$
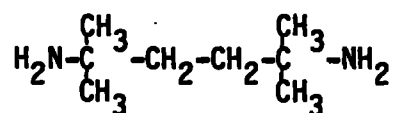
which is a relatively flexible molecule with a sterically crowded C atom adjacent to the NH_2 group fulfills these requirements.[4,5] The DGEBA-DMHDA epoxy system exhibits long gel-times and low η's at 23°C. The P.A.-E reaction is ~50X faster than the S.A.-E reaction. Full cure can be attained within 3h at 100°C and 90% epoxide consumption can occur even at 60°C after 120h. This epoxy system is ductile in the 23-125°C temperature range and exhibits a T_g of 143°C.

C. PROCESSING AND CHEMICAL STRUCTURE OF TGDDM-DDS EPOXIES USED IN COMPOSITES FABRICATED FROM PREPREGS.

C.I. INTRODUCTION

Diaminodiphenyl sulfone (DDS) cured tetraglycidyl 4,4'diaminodiphenyl methane (TGDDM) epoxies are the most common composite matrices utilized in high performance fibrous composites prepared from prepregs. The structures of the unreacted TGDDM epoxide and DDS monomers are illustrated in Fig. 3. The TGDDM epoxide monomer is a liquid at 23°C, whereas the DDS monomer is a crystalline powder with a m.p. of 162°C. The commercially available prepreg resins such as Narmco 5208, Fiberite 934 and Hercules 3501, all primarily consist of the TGDDM-DDS epoxy; the latter two systems also contain boron trifluoride catalysts.[6-8]

To manufacture reproducible C-fiber-TGDDM-DDS epoxy composites with well-defined lifetimes in service environment requires a knowledge of the parameters that affect composite processing conditions and the resultant structure of the epoxy within the composite. The cure reactions directly control the composite processing and the final epoxy network structure and mechanical response. Hence, it is important to understand the cure reactions and the variables that affect such reactions.

In this section we describe the starting material impurities and their effect on the processing and cure reactions of TGDDM-DDS epoxies. The cure reactions are characterized by differential scanning calorimetry (DSC) and Fourier transform infrared spectroscopy (FTIR)

studies. The BF_3:amine catalysts used to accelerate the cure of TGDDM-DDS epoxies are characterized by nuclear magnetic resonance (NMR) spectroscopy studies.

C.II. STARTING MATERIALS-IMPURITIES

The commercially available TGDDM, DDS and BF_3:amine components all contain impurities, some of which may act as catalysts towards the cure reactions.

FTIR studies indicate that commercial TGDDM (MY720, Ciba Geigy) contains 15-20% less epoxide groups than the pure tetrafunctional TGDDM epoxide molecule.[9-11] Liquid chromatography studies indicate that the missing -CH_2-$\overset{O}{\overset{\triangle}{CH}}$-$CH_2$ epoxide groups are replaced by (i) -CH_2-CH(OH)-CH_2(OH), (ii) -CH_2-CH(OH)-CH_2Cl, (iii) -H, (iv) -CH_3 and (v) -CH=CH-CH_2Cl groups with the α-glycol being the predominant impurity species.[12-14] In addition higher oligomers and homopolymer species may also be present. Pearce et al,[13] Hagnauer and Pearce[14] and Scola[15] report that the epoxide groups in TGDDM can hydrolyze to the α-glycol species and that such species catalyze homopolymerization reactions.

Commercial DDS also contains a small percentage of a crystalline impurity as indicated by a DSC endotherm at 77°C whose heat of fusion is 3% of the total heat of fusion associated with the pure DDS m.pt at ~ 165°C.[16]

The impurities in the BF_3:amine catalysts are highly variable and are discussed in detail in the following section C.III.

C.III. <u>NMR CHARACTERIZATION OF BF$_3$:AMINE CATALYSTS</u>

(1) <u>Introduction</u>

The cure reactions, the viscosity-time-temperature profile, the processing conditions, the resultant epoxy chemical and physical structure, and the mechanical response of a C-fiber/TGDDM-DDS cured epoxy composite are modified by the presence of a BF$_3$-amine complex catalyst within the prepreg. These factors also will be modified by the distribution of the catalyst within the prepreg, its chemical composition, and any modification of its structure and activity as a result of exposure to or interactions with heat or both, moisture, and the epoxide and amine components within the prepreg.

The two most common BF$_3$:amine catalysts used commercially to cure epoxies are boron trifluoride monoethylamine, BF$_3$:NH$_2$C$_2$H$_5$, and boron trifluoride piperidine, BF$_3$:NHC$_5$H$_{10}$, complexes. Such complexes are latent catalysts at room temperature but enhance epoxide group reactivity at higher temperatures.

In this section we discuss ^{1}H, ^{19}F and ^{11}B NMR studies of BF$_3$:NH$_2$C$_2$H$_5$ and BF$_3$:NHC$_5$H$_{10}$ complexes, with principal emphasis on the former. We present the chemical composition of commercial BF$_3$:amine complexes, their thermal stability in the solid state and in solution, the effect of moisture and heat upon their composition, the nature of their interaction with the epoxide and amine components utilized in TGDDM-DDS commercial prepregs, the composition of BF$_3$:amine complexes in commercial prepregs, their thermal stability in the prepregs, and the chemical structure of the predominant catalytic species of the cure reactions of the prepreg.

(ii) Chemical Composition

The ^{1}H NMR spectrum of $BF_3:NH_2C_2H_5$ should exhibit peaks in three separate regions, namely, the CH_3 region at highest field, the CH_2 region at an intermediate field, and the NH_2 region at lowest field. The theoretical peak intensity distribution should be 3:2:2 for the CH_3,CH_2, and NH_2 regions, respectively. The ^{1}H NMR spectra for the four $BF_3:NH_2C_2H_5$ samples are illustrated in Fig. 4. Two components were observed in the spectra. The major component spectra consisted of a CH_3 triplet (1.090 ppm), a CH_2 quartet (2.612 ppm), and an NH_2 signal (6.156 ppm). The intensity ratios were 3:2:2, respectively, and this spectrum was assigned to the $BF_3:NH_2C_2H_5$. A second component was evident in the proton NMR spectra, characterized again by a CH_3 triplet (1.121 ppm), a CH_2 quartet (2.803 ppm), and an NH/OH peak from labile protons (7.27 to 7.63 ppm). Intensity ratios were 3:2:3. This spectrum is attributed to $(BF_4^-$ or $BF_3OH^-)$ $NH_3^+C_2H_5$ species. The proton intensity measurements indicate that BF_4^- is the dominant anion.

The ^{19}F NMR spectra of the commercial $BF_3:NH_2C_2H_5$ samples are illustrated in Fig. 3. The major components identified in the ^{19}F spectra were $BF_3:NH_2C_2H_5$, BF_4^-, and $BF_3(OH)^-$ species and an unidentified highly reactive BF_3 species with an NMR peak in the region of $BF_3(OH)^-$. The fluorine species observed in the commercial samples are illustrated in Table 1, in which several other observed ^{19}F NMR peaks are combined under the "Miscellaneous" heading.

The chemical composition of a $BF_3:NHC_5H_{10}$ sample was also investigated by ^{19}F NMR. Three fluorine-containing environments were found with fluorine distributed as follows: $BF_3:NHC_5H_{10}$ (87.3%), BF_4^--$NH_2^+C_5H_{10}$ (11.5%), and $BF_3(OH)^-$ $NH_2^+C_5H_{10}$ (0.2%).

Table 1. Fluorine species in $BF_3:NH_2C_2H_5$ from ^{19}F NMR.

	Percent Total Fluorine as				
Source	$BF_3:NH_2C_2H_5$	BF_4^-	$BF_3(OH)^-$	Reactive BF_3	Miscel-laneous
Alfa	92.5	2.5	2.9	2.0	0.1
Pfaltz and Bauer	1.9	15.3	12.4	57.3	13.1
Harshaw	89.7	8.9	0.9	-	0.5
K. and K.	78.1	11.1	3.1	4.8	2.9

(iii) Thermal Stability

Solid $BF_3:NH_2C_2H_5$ samples that were annealed at 85, 115, or 139°C for 1 h and then subsequently dissolved in dimethyl sulfoxide (DMSO) exhibited no significant dissociation as detected by [1]H. These data are consistent with observations by Harris and Temin[18] that $BF_3:$amine complexes do not dissociate irreversibly to gaseous BF_3 and amine products. (The $BF_3:NH_2C_2H_5$ was observed to melt near 85°C during these studies.)

However, ^{19}F NMR studies indicate that a small amount of the

$BF_3:NH_2C_2H_5$ may slowly convert to BF_4^- and to another species which we do

not detect in the ^{19}F spectrum. There is an apparent loss of fluorine

as illustrated in Table 2. The small percentage of $BF_3(OH)^-$ species

present in the unannealed sample disappears after a 1-h annealing at

85°C, presumably as a result of either reaction with species at the

glass sample tube surface or formation of

Table 2. ·Effect of thermal annealing on the fluorine species
in $BF_3:NH_2C_2H_5$ from ^{19}F NMR

Annealing Conditions	Percent Total Original Fluorine			
	Fluorine Loss	$BF_3(OH)^-$	BF_4^-	$BF_3:NH_2C_2H_5$
Original (unannealed solid)	0	6.1	1.6	92.3
1 h at 85°C	8.1	0	11.8	80.1
1 h at 115°C	2.7	0	13.8	83.5
1 h at 140°C	9.7	0	13.7	76.6

species which undergo chemical exchange at an intermediate rate on the

NMR time scale.

If $BF_3:NH_2C_2H_5$ is heated directly in DMSO, the conversion to BF_4^-

and the percentage fluorine loss is considerably greater than if

$BF_3:NH_2C_2H_5$ is heated on the absence of the solvent, as illustrated in

Table 3. The conversion of the $BF_3:NH_2C_2H_5$ to BF_4^- species with

associated fluorine loss could perferentially occur at the glass sample

tube surface. Hence, such reactions would be accelerated in solution

because the mobility of the $BF_3:NH_2C_2H_5$ is enhanced. However, we cannot rule out the possibility of a reaction between the $BF_3:NH_2C_2H_5$ and the DMSO solvent that enhances conversion to BF_4^- species.

$BF_3:NHC_5H_{10}$ exhibits similar thermal stability trends as $BF_3:NH_2C_2H_5$.

Table 3. Effect of heating on the fluorine species in $BF_3:NH_2C_2H_5$ DMSO solution from ^{19}F NMR.

| Heat Conditions | Percent Total Original Fluorine as | | | |
	Fluorine Loss	$BF_3(OH)^-$	$BF_3:$ BF_4^-	$NH_2C_2H_5$
Unheated solution	0	6.1	1.6	92.3
1 h at 85°C	5.1	0	13.1	81.8
1 h at 115°C	12.9	0	34.7	52.4
1 h at 140°C	27.3	0	60.2	12.5

(iv) Hydrolytic Stability

^{19}F NMR studies of $BF_3:NH_2C_2H_5$/DMSO solutions indicated that little change occurred in the amount of $BF_3:NH_2C_2H_5$, BF_4^-, and $BF_3(OH)^-$ species in the presence of added H_2O over a period of 4 days at 23°C.

However, if a large (ten-fold) excess of H_2O was added to the $BF_3:NH_2C_2H_5$/DMSO solution and the temperatures raised to 85°C for 1 h, the amount of fluorine present as $BF_3:NH_2C_2H_5$ decreased by 50% while that present as $BF_3(OH)^-$ $NH_3^+C_2H_5$ increased from 5 to 40%. The more stable BF_4^- species were unaffected.

The $BF_3NHC_5H_{10}$ species in DMSO behaved similarly to the corresponding $BF_3:NH_2C_2H_5$ species upon exposure to H_2O at 23 and 85°C.

(v) Interaction of $BF_3:NH_2C_2H_5$ with DDS and TGDDM

^{1}H and ^{19}F NMR were used to study the interaction of the individual resin components of the C-fiber/TGDDM-DDS prepregs with $BF_3:NH_2C_2H_5$.

It was determined that the ^{1}H NMR spectrum of DDS in DMSO does not change when $BF_3:NH_2C_2H_5$ is added at ambient temperature. $BF_3:NH_2C_2H_5$/DDS/DMSO solutions were then monitored after heating for 1 h at 85, 115, or 139°C. The broad CH_2 multiple associated with $BF_3:NH_2C_2H_5$ in the proton spectra decreased with increasing temperature exposure, ultimately resulting in a sharp CH_2 quartet which is associated with either BF_4^- $NH_3^+C_2H_5$ or $BF_3(OH)^-$ $NH_3^+C_2H_5$ species.

^{19}F NMR studies also indicate that significant changes in the BF_3 species occur upon heating $BF_3:NH_2C_2H_5$/DDS/DMSO solutions. The degree of conversion to the BF_4^- salt, for the same thermal exposure, is similar to that observed in $BF_3:NH_2C_2H_5$/DMSO solution (Table 3) in the absence of DDS. Hence, we have no direct evidence that DDS competes with $C_2H_5NH_2$ for BF_3 molecules or that DDS enhances BF_4^- salt formation upon heating in DMSO solution.

The ^{1}H NMR spectra of $BF_3:NH_2C_2H_5$/TGDDM/DMSO solutions were investigated as a function of thermal exposure. Heating the solution for 1 h at 85°C did not produce changes in the ^{1}H spectra. However, exposures to 115 or 139°C for 1 h did produce significant spectral changes. The unmodified TGDDM ^{1}H NMR spectrum contains two doublets

centered at 7.022 and 6.763 ppm which are associated with the two types of aromatic protons. The five different chemical proton environments associated with the

$$N-CH_2-\overset{O}{\overset{\triangle}{CH}}-CH_2$$
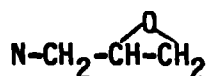
group result in the series of peaks in the 2.500- to 3.500-ppm region. We have not attempted to assign peaks in this region to specific proton environments. The essential disappearance of the TGDDM aromatic proton doublets and the modification of the spectral region associated with the TGDDM aliphatic protons after heating for 1 h at 115 and 139°C confirms that $BF_3:NH_2C_2H_5$ reacts extensively with the TGDDM epoxide.

^{19}F NMR studies, illustrated in Table 4, indicate that the TGDDM epoxide enhances BF_4^- salt formation in DMSO solution. For example, after exposure to 115°C for 1 h, all the $BF_3:NH_2C_2H_5$ species have disappeared in the presence of TGDDM. However, in DMSO solution in the absence of TGDDM, 50% of the total fluorine species are still in the form of $BF_3:NH_2C_2H_5$ after 1 h exposure at 115°C (Table 3).

Table 4. Effect of heating on the fluorine species in $BF_3:NH_2C_2H_5/$ TGDDM/DMSO solution from ^{19}F NMR.

| Heat Conditions | Percent Total Original Fluorine as | | | |
	Fluorine Loss	$BF_3(OH)^-$	BF_4^-	$BF_3:NH_2C_2H_5$
Unheated solution	0	6.1	1.6	92.3
1 h at 85°C	19.4	0	17.8	62.8
1 h at 115°C	23.0	0	77.0	0
1 h at 140°C	20.6	0	79.4	0

(vi) <u>Catalyst Composition in Prepregs</u>

The catalyst composition in Fiberite 934 and Hercules 3501 prepregs was investigated by ^{19}F NMR. The epoxy resin in these commercial C-fiber/TGDDM-DDS prepregs was dissolved in DMSO.

The fluorine species observed in five different lots of Fiberite 934 were identified and tabulated in Table 5. A typical spectrum is illustrated in Fig. 6. The catalyst in this prepreg was identified as $BF_3:NH_2C_2H_5$ by ^{19}F NMR. There is considerable variation from lot to lot in the $BF_4^-NH_3^+C_2H_5$ (14.6 to 60.0%) and the $BF_3:NH_2C_2H_5$ (7.2 to 48.6%) species.

Table 5. - Fluorine species in Fiberite 934 lots

Lots	$BF_3(OH)^-$ $NH_3^+C_2H_5$	$BF_4^-NH_3^+$ C_2H_5	$BF_3:NH_2C_2H_5$	Epoxide-BF_3 Products
C2-709	3.8	38.8	25.2	32.2
C3-218	4.6	60.0	7.2	28.2
C3-389	0.5	14.6	48.6	36.3
C3-397	1.5	44.4	22.4	31.7
C3-546	1.4	49.1	18.2	31.3

We associate the various additional fluorine peaks observed in the NMR spectra with principally the products of epoxide-active fluorine species reactions. The total fluorine in the form of these products is relatively constant from prepreg lot to lot (28.2 to 36.3%).

The epoxy resin of a Hercules 3501 sample was dissolved in DMSO and investigated by ^{19}F NMR. The ^{19}F peaks associated with $BF_3:NH_2C_2H_5$ were absent and the 1:1:1:1 quartet associated with $BF_3:NHC_5H_{10}$ was found at an ^{19}F chemical shift value of - 155.17 ppm. The fluorine distribution among species found in this sample was $BF_3(OH)^-$ $NH_2^+C_5H_{10}$ (2.8%). BF_4^- $NH_2^+C_5H_{10}$ (9.9%), $BF_3:NHC_5H_{10}$ (78.3%), and epoxide-fluorine products (9.0%).

The Fiberite 934 prepreg was exposed to a series of temperature-time profiles and the soluble epoxy resin portion dissolved in DMSO and studied by ^{19}F NMR. The ratios of the intensity of the peak associated with $BF_3:NH_2C_2H_5$ (I_{BF_3}) to that intensity of the $BF_4^-NH_3^+C_2H_5$) ($I_{BF_4^-}$) species as a function of exposure conditions are tabulated in Table 6. With increasing annealing temperature, the $BF_3:NH_2C_2H_5$ species concentration decreases relative to the BF_4^- $NH_3^+C_2H_5$ species. The presence of steam slows the relative disappearance of the $BF_3:NH_2C_2H_5$ species.

Table 6. The effect of temperature, time, and H_2O
on the relative extractable $BF_3:NH_2C_2H_5$
and BF_4^- $NH_3^+C_2H_5$ species in Fiberite 934.

Exposure Conditions	$I_{BF_3}/I_{BF_4^-}$
Ambient	0.718,0.748
1 h at 50°C	0.539
5 h at 50°C	0.554
1 h at 75°C	0.494
1 h at 100°C	0.146
1 h at 100°C + steam	0.326

(vii) <u>Catalytic Species and Activity</u>

Our NMR studies indicate that $BF_3:NH_2C_2H_5$ is slowly converted to $BF_4^- NH_3^+C_2H_5$ salt with corresponding loss of fluorine upon heating and solid catalyst. This conversion to the salt is accelerated in DMSO solution and further accelerated in TGDDM/DMSO solutions with an associated 20 to 30% loss of fluorine upon near-complete conversion to the salt. We will now consider the catalytic mechanism and activity of $BF_3:NH_2C_2H_5$ toward the TGDDM-DDS cure reaction in the light of our NMR observations.

The $BF_3:NH_2C_2H_5$ can react directly with an epoxide resulting the formation of a monoboroester and HF

$$BF_3-NH_2C_2H_5 + R-CH-CH_2 \rightarrow$$

(2)
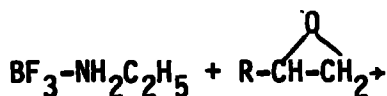
$$R-CH-CH_2-NH-C_2H_5 + HF$$
$$\overset{OBF_2}{|}$$
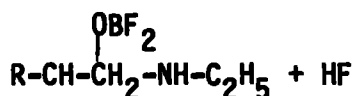
The HF generated then reacts with another $BF_3:NH_2C_2H_5$ to form the salt

$$BF_3-NH_2C_2H_5 + HF \rightarrow BF_4^-NH_3^+C_2H_5 \qquad (3)$$

The HF can also react with the components of the prepreg resulting in a variety of carbon-fluorine containing species. The formation of the BF_4^- salt requires two $BF_3:NH_2C_2H_5$ molecules to be in close proximity.

Hence, the formation of the BF_4^- salt will intimately depend on the dispersion of the small quantity (0.4 wt%) of the $BF_3:NH_2C_2H_5$ catalyst within the prepreg and, therefore, could be highly variable. The monoboroester can act as a catalyst for the cure reactions[19] but is susceptible to deactivation by hydrolysis.

All BF_3 and BF_3-prepregs species, with the exception of the BF_4^- $NH_3^+C_2H_5$ salt are susceptible to transformation to less active or nonactive catalytic species. Furthermore, our NMR results indicate that the $BF_4^-NH_3^+C_2H_5$ salt does not irreversibly, chemically react with the prepreg components.

For each epoxide group to be catalyzed by a BF_3 species in a prepreg containing 0.4 wt% $BF_3:NH_2C_2H_5$ catalyst requires each catalytic species to act as a catalyst to 200 epoxide groups. This means each BF_3 catalytic species has to be chemically stable and mobile. Hence, we suggest that the BF_4^- $NH_3^+C_2H_5$ salt is the predominant catalytic species for the prepreg cure reactions, with the more active BF_3 species becoming deactivated or immobilized during the early stages of cure. Harris and Temin[18] have reported that BF_3-amine complexes and their corresponding BF_4^- salts cure epoxides in the same temperature range and cure times. This observation is consistent with the BF_4^- salt being the predominant catalytic species and the BF_3-amine complex converting to the BF_4^- salt in the presence of epoxide groups.

C.IV.DSC STUDIES OF THE CURE REACTIONS

(i) Introduction

In C-fiber-TGDDM-DDS prepregs that do not contain a BF_3:amine catalyst one exotherm peak associated with the cure reactions has been observed by DSC.[20-22] However, prepregs that contain BF_3:amine catalyst have been reported to exhibit 2 or 3 additional DSC peaks at lower temperatures, which have been associated with the catalyzed cure reactions.[20,23]

In this section we report systematic DSC studies of (i) the constituents of boron trifluoride monoethylamine (BF_3:$NH_2C_2H_5$) catalyzed TGDDM-DDS epoxies and their mixtures; (ii) the nature of the catalyzed cure reactions and (iii) the environmental sensitivity of the BF_3:$NH_2C_2H_5$ catalyst. DSC studies are also reported on the cure reaction characteristics and environmental sensitivity of commercial prepregs that contain BF_3:amine catalysts.

(ii) Prepreg Mixtures and their Components

In Figs. 7(a) and (b) DSC plots are compared for a standard TGDDM (64 wt%)/DDS (25 wt%)/DGOP (11 wt%) commercial prepreg mixture containing 0 and 0.4% of the BF_3:$NH_2C_2H_5$ catalyst respectively. (DGOP is a diglycidyl orthophthalate epoxide, Gly-Cel-A-100, Celanese). In the absence of the BF_3:$NH_2C_2H_5$ catalyst (Fig. 7(a)) a large exotherm occurs at 240°C (ΔH = 470 j/g) with a smaller exotherm at 125°C (ΔH = 30 j/g),

whereas upon addition of the catalyst (Fig. 7(b) 4 peaks designated α, β, γ and δ are present at 240°C (ΔH = 210 j/g); 200°C (ΔH = 190 j/g); 160°C (ΔH = 70 j/g) and 125°C (ΔH = 25 j/g) respectively.

In an effort to characterize the chemical reactions associated with each peak, DSC runs were performed on each of the constituents of the epoxy prepreg and systematic 2, 3 and 4 constituent mixtures. (The constituent mixtures were formulated at the same relative compositions that were present in a standard epoxy prepreg mixture). The ΔH values and temperatures associated with maximum peak intensity for each DSC peak for each component and epoxy prepreg mixture were determined and are plotted in Fig. 8. The DSC peaks are represented by lines in the ΔH-temperature plots in Fig. 8, with the magnitude of each line representing the ΔH value associated with each peak, and its position on the temperature scale representing the temperature of maximum peak intensity. All line magnitudes represent exotherm peaks with the exception of the DDS and $BF_3:NH_2C_2H_5$ endotherm m.pts. which are designated by negative symbols ⊖② and ⊖④ respectively. The five ΔH-temperature plots in Fig. 8 represent, from the top to the bottom of the Figure, 1, 2, 3 and 4 component prepreg mixtures and Fiberite 934 respectively. From this systematic study illustrated in Fig. 8 we conclude the α peak at 240°C is associated with the non-catalyzed cure reactions and the β, γ and δ peaks with $BF_3:NH_2C_2H_5$ catalyst-epoxy prepreg constituent reactions.

The ΔH values associated with the α, β and γ peaks are plotted as a function of $BF_3:NH_2C_2H_5$ catalyst concentration in Fig. 9. The α peak intensity associated with non-catalyzed cure reactions progressively decreases with increasing $BF_3:NH_2C_2H_5$ concentration and approaches zero

near 2 wt.% $BF_3:NH_2C_2H_5$. The γ peak intensity progressively increases with $BF_3:NH_2C_2H_5$ concentration, whereas the β peak intensity attains a maximum intensity at ~0.4 wt.% $BF_3:NH_2C_2H_5$ and then decreases with higher concentrations of $BF_3:NH_2C_2H_5$. The small δ peak intensity does not appear to be modified by increasing $BF_3:NH_2C_2H_5$ concentration.

From these DSC studies together with our NMR observations from Section C. III. we conclude (i) the δ peak is associated with $BF_3:NH_2C_2H_5$ catalyzed DDS-TGDDM impurity reactions; (ii) the γ peak is associated $BF_3:NH_2C_2H_5$ and monofluroborate catalyses of the cure reactions and (iii) the β peak is associated $BF_4^-NH_3^+C_2H_5$ cationic catalyses of the cure reactions.

(iii) Environmental Sensitivity of $BF_3:NH_2C_2H_5$ Catalyst

There are reports in the literature of H_2O deactivating the catalytic activity of $BF_3:NH_2C_2H_5$.[24,25] Our NMR studies[17] indicate that $BF_3:NH_2C_2H_5$ can hydrolyze to form the hydroxy fluoroborate salt, particularly at more extreme conditions of 85°C. DSC peak intensities indicate that when the $BF_3(OH)^-NH_3^+C_2H_5$ salt is substituted for $BF_3:NH_2C_2H_5$ in a TGDDM/DDS prepreg mix the cure reactions are not modified. This suggests that the $BF_3(OH)^-NH_3^+C_2H_5$ dehydrates back to $BF_3:NH_2C_2H_5$ during the early stages of cure. However, exposure of the Fiberite 934 prepreg to 85°C for 1 h at 100% RH does produce a significant shift in the intensities of the DSC peaks with the γ peak intensity decreasing by ~50% and the α peak intensity increasing by 50%. We suggest that during the environmental exposure conditions we may have leached a portion of the $BF_3:NH_2C_2H_5$ catalyst out of the prepreg, as we have observed the catalyst is readily soluble in H_2O.

(iv) Commercial Prepregs

We investigated the variability in catalyst activity within a Fiberite 934 lot and also between different lots by monitoring the magnitude of the ΔH values associated with the α, β and γ DSC peaks. The ΔH values associated with each peak varied by only $\pm 5\%$ for samples within close proximity of each other (<10 cms apart) within a prepreg lot. However, the variability in ΔH values was considerably greater (up to $\pm 30\%$) for samples investigated from (i) the same prepreg lot that were widely separated (>20 cm apart) and (ii) between different prepreg lots.

From DSC ΔH peak intensities we ascertained that on the average Fiberite 934 prepreg cure reactions occur (i) 25% by non-catalyzed reactions (αpeak), (ii) 50% $BF_4^- NH_3^+ C_2H_5$ catalyzed reactions (βpeak) and (iii) 25% by $BF_3:NH_2C_2H_5$ catalyzed reactions (γpeak). From similar DSC studies on the Hercules 3501 prepreg we concluded the cure reactions occur (i) 75% by $BF_4^- NH_2^+ C_5H_{10}$ catalyzed reactions and (ii) 25% by $BF_3:NHC_5H_{10}$ catalyzed reactions. In both commercial prepregs the δpeak is absent, because the $BF_3:$amine catalyzed DDS-TGDDM impurity reactions have already occurred during the epoxy mixing and C fiber-prepreg processing conditions.

C.V. FTIR STUDIES OF THE CURE REACTIONS

(i) Introduction

To consume all epoxide groups in the TGDDM-DDS epoxy system exclusively by P.A.-E and S.A.-E addition reactions would require 37 wt% DDS. However, commercial TGDDM-DDS epoxy systems contain only 20-25 wt% DDS. Thus, other reactions as well as epoxide-amine addition reactions must occur to consume all the epoxide groups in these systems.

In this section we report systematic FTIR studies of the cure reactions of TGDDM-DDS epoxies. We report our cure and degradation reaction studies of TGDDM-DDS epoxies from 100 to 300°C as a function of cure time and DDS and $BF_3:NH_2C_2H_5$ concentration.[9-11,26,27]

(ii) TGDDM Epoxide Hompolymerization

The homopolymerization reactions of impure TGDDM (MY720) in the presence and absence of a $BF_3:NH_2C_2H_5$ catalyst and, also, pure TGDDM were monitored by FTIR as a function of cure temperature from 177 to 300°C. The intensities of the epoxide, hydroxyl, ether and carbonyl bands at 906, 3500, 1120 and 1720 cm^{-1} respectively were determined from spectral differences and are plotted as a function in cure conditions in Figs. 10, 11, 12 and 13 respectively. The 906, 1120 and 1720 cm^{-1} band intensities were normalized to the 805 cm^{-1} band and the 3500 cm^{-1} to the 1615 cm^{-1} band. The 805 and 1615 cm^{-1} bands are associated with the phenyl group which is assumed to be chemically unmodified during the homopolymerization reactions.

Epoxide consumption, Fig. 10, primarily occurs in the 175-250°C range with the rate of epoxide consumption being $MY720-BF_3:NH_2C_2H_5$ >MY720> pure TGDDM. In agreement with previous observations,[13-15] the impurities in MY720 enhance epoxide consumption relative to pure TGDDM.

Ether, hydroxyl and carbonyl band intensities (Figs. 11, 12, and 13) simultaneously increase in the same temperature range as the epoxide band intensity decreases (Fig. 10). The carbonyl band appears to be directly correlated to epoxide consumption rather than general oxidation reactions because the carbonyl band intensity does not increase once the epoxide groups are all consumed. The intensities of the ether, hydroxyl and carbonyl bands decrease with increasing temperature in the 225-300°C range as a result of network degradation.

In the 177-300°C temperature range studied, epoxide isomerization, oxidation and homopolymerization can occur followed by complex degradation reactions. There have been numerous studies on the homopolymerization of epoxides including the effects of catalysts, alcohols, cure temperature and epoxide-amine ratio on the chain extension reactions.[13,14,20,28-49] The appearance of hydroxyl, ether and unsaturation have been reported during homopolymerization of epoxides.[30,37,40]

There is considerable evidence in the literature that chain extension reactions can occur between epoxide and hydroxyl groups and that this reaction (4) is enhanced in the presence of the tertiary amines.[28,29,32,36,40,42-48,50] In the case of TGDDM

$$R_1CH_2\overset{O}{\overset{\diagup\diagdown}{CH-CH_2}} + R_2OH \rightarrow R_1CH_2-\overset{OH}{\overset{|}{CH}}-CH_2OR_2 \qquad (4)$$
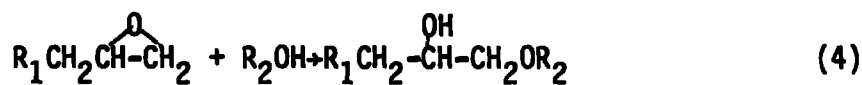
homopolymerization, hydroxyl groups are present in the impure TGDDM (MY720) as α-glycol groups and further hydroxyl groups can form in the 177-300°C range as a result of isomerization and/or oxidation of the epoxide groups. The presence of the tertiary nitrogen NR_3 groups in the TGDDM molecule should enhance the epoxide-hydroxyl (E-OH) reaction. The hydroxyl groups present in MY720 accelerate the rate of epoxide consumption compared to pure TGDDM, which indicates that the E-OH reactions rather than epoxide-epoxide (E-E) reactions are the predominant chain extension reactions for TGDDM.

A number of workers have reported epoxides isomerize to allylic alcohols (5).[30,35-38,40,41,51-56] Epoxide isomerization to

$$R-CH_2-CH-CH_2 \rightarrow R-CH_2-C=CH_2 \text{ or } R-CH=CH-CH_2OH \qquad (5)$$
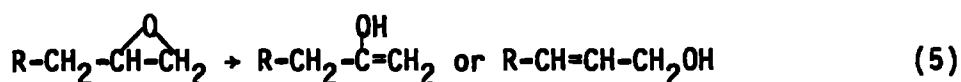
allylic alcohols and also to an aldehyde (6) is consistent with the simultaneous appearance of hydroxyl and carbonyl groups upon epoxide consumption. The absence of a methyl

$$R-CH_2-CH-CH_2 \rightarrow R-CH_2CH_2-CHO \qquad (6)$$

group in the IR spectra indicates isomerization to an aldehyde rather .than a ketone is preferred.

In addition to isomerization some of the epoxide groups could be oxidized to hydroxyl aldehyde and then carboxylic acid groups (7).[57] These oxidation reactions would also be consistent with our FTIR observations.

$$R-CH_2-CH-CH_2 \xrightarrow{O_2} R-CH_2CH-C\begin{smallmatrix}O\\H\end{smallmatrix} \xrightarrow{O_2} R-CH_2CH-C\begin{smallmatrix}O\\OH\end{smallmatrix} \qquad (7)$$
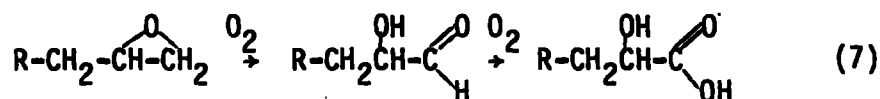
Hence, the most plausible explanation of our FTIR observations of the simultaneous appearance of hydroxyl, carbonyl and ether groups upon TGDDM epoxide consumption is epoxide isomerization and/or oxidation followed by epoxide-hydroxyl chain extension reactions.

At the higher temperature range of our studies, 225-300°C, degradation reactions of the polymerized network will occur. Previous studies on the degradation of epoxies indicate dehydration will be the principal degradation mecahnism in the 225-300°C temperature range over time periods of hours[36,58-63] which is consistent with the observed decrease in hydroxyl band intensity with increasing temperature in this range.

(iii) TGDDM-DDS Cure Reactions

In this section we report FTIR studies of the cure reactions of TGDDM-DDS-BF_3:$NH_2C_2H_5$ epoxy systems as a function of cure conditions (100-300°C) and DDS (0-35 wt%) and BF_3:$NH_2C_2H_5$ (0-5 wt%) concentrations. We monitored by FTIR difference spectra the disappearance of the epoxide and P.A. groups and the appearance of the S.A., ether and hydroxyl groups. The I.R. bands at 1630 and 3410 cm^{-1} were assigned to the P.A. and S.A. groups respectively and their intensities normalized relative to the 1516 cm^{-1} band associated with the phenyl group. The intensity of S.A. group was further normalized against the O=S=O band from the DDS structure ($I_{NH:SO_2}$) which we assume does not change in intensity during

cure. This normalization allows comparison of S.A. changes independent of the effects of DDS concentration. We, also, normalized the OH and ether IR band intensities relative to the initial epoxide band intensity by the following expression, illustrated in this case for the OH band intensity, where R_{OH}, IOH_T, $IOH_{23°C}$, $IE_{23°C}$

$$R_{OH} = \frac{IOH_T - IOH_{23°C}}{IE_{23°C} \times (M.F.)_{TGDDM}} \tag{8}$$

and (M.F.) TGDDM are the normalized OH band intensities at cure temperature T and 23°C, epoxide band intensity at 23°C and the mole fraction of epoxide groups relative to pure TGDDM, respectively. The disappearance of the epoxides and P.A.'s in %'s and the appearance of the S.A.'s, OH's and ethers in the form of $I_{NH:SO_2}$, R_{OH} and R_{ether} values respectively are plotted in Fig. 14 as a function of cure time at 177°C for a TGDDM-DDS (25 wt%)-$BF_3:NH_2C_2H_5$ (0.4%) epoxy system. After 210 mins at 177°C 85% of the epoxide groups are consumed. At the latter stages of cure the epoxide consumption rate is evidently hindered by steric restrictions. The P.A.-E reaction dominates th early stages of cure. After 30 mins at 177°C, 95% of P.A. groups and 45% of the epoxide groups have reacted; 28% of these epoxide groups are consumed by the P.A.-E reaction. From FTIR and DSC studies of the cure of a non-$BF_3:NH_2C_2H_5$ catalyzed TGDDM-DDS epoxy at 177° Moacanin et al[64] and Gupta et al[22] have concluded the P.A.-E reaction dominates the early stages of cure. Also, chemical titration and liquid chromatography studies[65] indicates epoxide consumption is linear with time during the early stages of cure which is also consistent with the predominance of the P.A.-E reaction.

In the 30-90 min. cure time range there is a 45% increase in the R_{OH} intensity, despite 95% of the P.A.'s being consumed after 30 min. This increase could be caused by ~25% of the S.A.'s reacting with 7% of the epoxides via S.A.-E addition reactions. The $I_{NH:SO_2}$ intensity decrease associated with the S.A.-E reaction would be difficult to detect because the P.A.-E reaction simultaneously causes an increase in this intensity. After 90 mins. of cure the R_{OH} and $I_{NH:SO_2}$ values remain constant with increasing cure time which indicates the S.A.-E reaction does not occur during the later stages of cure probably because of network steric restrictions. The S.A.-E reaction rate constant for aromatic amines with structures similar to DDS, such as methylene dianiline, have been reported to be 7-12 times slower than for the P.A.-E reaction.[66]

The increase in the R_{ether} through-out the cure is associated with the E-OH reaction which consumes ~50% of the total epoxides.

The cure reactions of TGDDM-DDS (25 wt%) epoxy were monitored as a function of $BF_3:NH_2C_2H_5$ concentration (0-5 wt%) in the 100-177°C cure temperature range. The cure reactions were accelerated with increasing $BF_3:NH_2C_2H_5$ concentration and shifted to lower cure temperatures.

The cure and degradation reactions of TGDDM-DDS epoxies were also monitored by FTIR in the 177-300°C as a function of DDS concentration (0-35 wt%). Three series of epoxies were studied containing (i) 0 wt% $BF_3:NH_2C_2H_5$, (ii) 0.4 wt% $BF_3:NH_2C_2H_5$ and (iii) 0.4 wt% $BF_3:NH_2C_2H_5$-acetone mixed.

In Fig. 15 we illustrate data for a TGDDM-DDS epoxy series (0 wt% $BF_3:NH_2C_2H_5$) in which the disappearance of the epoxides and P.A.'s in %'s and the appearance of the S.A.'s, OH's and ethers in the form of

$I_{NH:SO_2}$, R_{OH} and R_{ether} values, respectively, are plotted as a function of DDS concentration and cure conditions. Similar plots were generated for the other two $BF_3:NH_2C_2H_5$ epoxy systems.
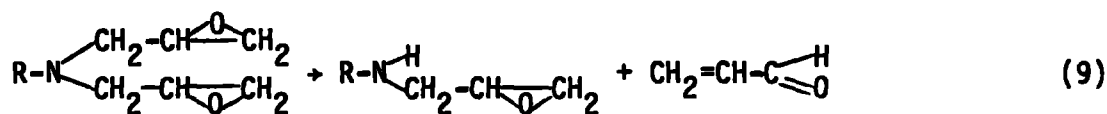
All P.A. groups are consumed at 177°C after 2.5 h cure for all TGDDM-DDS epoxy systems studied that contain <35 wt% DDS. For TGDDM-DDS (35 wt% DDS) epoxies, however, ~5% of P.A.'s remain unreacted even at 300°C, which suggests that these unreacted groups become inaccessible to epoxide groups during the later stages of cure because of network topography constraints.

In Fig. 16, plots of epoxide consumptions at 177°C after 2.5 h vs wt% DDS for all TGDDM-DDS systems studied are illustrated. From these data and similar plots at higher cure temperatures we conclude: (i) At 177°C for a 2.5h cure for TGDDM-DDS (0.5 wt% DDS) epoxies, the $BF_3:NH_2C_2H_5$ catalyst enhances epoxide consumption 2-4 times. (ii) At cure temperatures in the 200-225°C range we found no definitive evidence that the $BF_3:NH_2C_2H_5$ catalyst enhances epoxide consumption for all systems studied, which suggests the principal catalytic species, the $BF_4^-NH_3^+C_2H_5$ salt, is deactivated in this temperature regime. (iii) At 177°C for TGDDM-DDS (15-35 wt% DDS) epoxies the $BF_3:NH_2C_2H_5$ catalyst enhances epoxide consumption, but does not always produce a fully cured system. The large scatter in these epoxide consumptions, 60-100%, from a number of experiments for the TGDDM-DDS (15-35 wt% DDS) epoxies, suggests there is a considerable variability in the $BF_3:NH_2C_2H_5$ catalytic activity. From our DSC and NMR studies of $BF_3:NH_2C_2H_5$ catalytic activity, we attribute the epoxide consumption data scatter to variability in inherent $BF_3:NH_2C_2H_5H$ chemical composition and its particle size distribution within the epoxy, and also non-uniform mixing
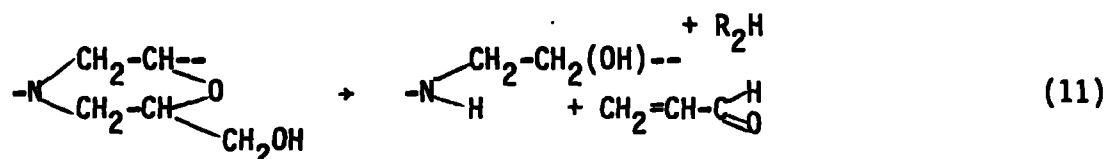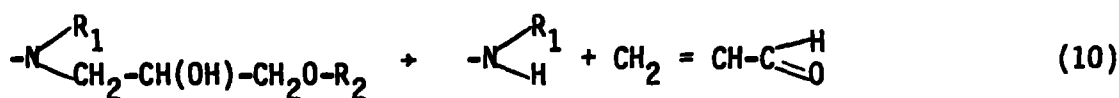
of this small concentration of catalyst in the epoxy. (iv) From two completely independent series of acetone and non-acetone mixed epoxies we found no difference in epoxide consumption within experimental scatter. (v) The epoxide consumption is enhanced with increasing DDS concentration to a greater extent than that associated with 100% completed P.A.-E and 50% completed S.A.-E reactions (Fig. 16). The hydroxyl products of the P.A.-E and S.A.-E reactions enhance epoxide consumption via E-OH reactions. From their DSC studies Mijovic et al[67] suggest the cure reactions of TGDDM-DDS epoxies are autocatalytic.

The $I_{NH:SO_2}$ intensity after 2.5 hrs cure at 177°C decreases with increasing DDS concentration for the three TGDDM-DDS systems studied, as illustrated in Fig. 17. For a TGDDM-DDS (25 wt% DDS) (0 wt% $BF_3:NH_2C_2H_5$) epoxy the $I_{NH:SO_2}$ intensity is 30-40% lower than the maximum intensity observed at lower DDS concentrations, thus suggesting ~1/3 of the S.A. groups do react with epoxide groups in commercial prepregs under standard cure conditions.

The $I_{NH:SO_2}$ intensity increases in the 177-225°C region, despite the completion of the P.A.-E cure reaction that would result in additional S.A. groups. This $I_{NH:SO_2}$ intensity increase is more pronounced for lower DDS concentration systems. From vaporization gas-chromatography/mass spectroscopy studies Grayson and Wolf[68] report propenal is the principal degradation product of a TGDDM-DDS (21 wt% DDS) (0 wt% $BF_3:NH_2C_2H_5$) epoxy system in the 125-215°C region. Propenal was not observed, however, when MY720 was heated in the same temperature region,[69] which discounts propenal was formed by unimolecular decomposition of unreacted epoxide groups (9).

$$R-N \underset{CH_2-CH \overset{\Large O}{\underset{O}{\diagdown}} CH_2}{\overset{CH_2-CH \overset{\Large O}{\diagup} CH_2}{}} \rightarrow R-N \underset{CH_2-CH \underset{O}{\diagdown} CH_2}{\overset{H}{}} + CH_2 = CH-C \overset{H}{\underset{O}{\diagdown}} \qquad (9)$$

Propenal and the S.A. group formation must form from decomposition of the P.A.-E, S.A.-E and E-OH cure reaction products. However, because we observe the S.A. group formation is most prevalent for low DDS concentration TGDDM-DDS epoxies, which contain a higher concentration of E-OH cure reaction products, then we suggest propenal and S.A. group formation most likely occurs by decomposition of non-cyclized (10) and cyclized (11) E-OH reaction products. (see next section Rates and Chemistry of Cure Reactions)

$$-N \underset{CH_2-CH(OH)-CH_2O-R_2}{\overset{R_1}{\diagup}} \rightarrow -N \underset{H}{\overset{R_1}{\diagup}} + CH_2 = CH-C \overset{H}{\underset{O}{\diagdown}} \qquad (10)$$

$$-N \underset{CH_2-CH \underset{CH_2OH}{\diagdown} O}{\overset{CH_2-CH--}{}} \rightarrow -N \underset{H \quad + CH_2=CH-C \overset{H}{\underset{O}{\diagdown}}}{\overset{CH_2-CH_2(OH)-- \quad + R_2H}{}} \qquad (11)$$

Similar decomposition mechanisms have been proposed by David[70] and Grayson and Wolf.[68]

The hydroxyl band intensities, plotted in the form of R_{OH} values decrease with increasing temperature above 200°C for epoxies containing 15-35 wt% DDS, which indicates these epoxies dehydrate in this temperature regime. For epoxies containing 0-10 wt% DDS dehydration is not evident until above 250°C because isomerization of unreacted epoxide groups causes an increase in the concentration of OH groups in the 177-250°C temperature range. The R_{OH} value for a 177°C, 2.5 h cure increases with increasing DDS concentration, as illustrated in Fig. 18, because of the enhancement of the P.A.-E and S.A.-E cure reactions with

increasing DDS concentration. No significant differences in the dehydration processes were observed for the three TGDDM-DDS epoxy series that were studied.

Ether formation can occur from the E-OH reaction. In Fig. 19(a), the R_{ether} value for a 177°C, 2.5 h cure increases with increasing DDS concentration in the 0-15 wt% DDS range because of the enhanced availability of OH groups from the P.A.-E and S.A.-E addition reactions. For > 15 wt% DDS concentrations, ether formation is not enhanced with increasing DDS concentrations because the competing epoxide-amine addition reactions consume the available epoxide groups. At 0 wt% DDS, the $BF_3:NH_2C_2H_5$ catalyst enhances ether formation ~5 times, but in > 0 wt% DDS epoxies, the $BF_3:NH_2C_2H_5$ catalyst has no detectable effect on ether formation for a 177°C, 2.5 h cure. At higher cure temperatures from 177 to 300°C R_{ether} values increase with increasing cure temperature, Fig. 19(b), as a result of dehydration, and/or network oxidation and resultant formation of ether crosslinks.

(iv) <u>Rates and Chemistry of Cure Reactions</u>

The reaction rates of the three principal cure reactions of TGDDM-DDS epoxies are as follows:

$$d(PA-E)/dt = k[PA][E]$$

$$d(SA-E)/dt = 0.1k[SA][E]$$

$$d(E-OH)/dt = 0.1k[OH][E]$$

The rate constants for the S.A.-E and E-OH reactions are 10 times slower than the rate constant for the P.A.-E reactions. From FTIR and DSC studies Moacanin et al[64] report the E-OH reaction is 10 times slower than the P.A.-E reaction at 177°C. We previously mentioned that the S.A.-E rate constant for aromatic amines similar to DDS, such as methylene dianiline have been reported to be 7-12 times slower than the P.A.-E reaction.[66]

In Fig. 20a plot of the % of epoxides consumed by each cure reaction vs total percent epoxide consumed for a TGDDM-DDS (25 wt% DDS) epoxy cured at 177°C is illustrated. The P.A.-E reaction dominates the early stages of cure, until all the P.A. is depleted. The E-OH reaction dominates the later stages of cure.

The P.A.-E reaction is illustrated in Fig. 21, with the sites for further cure reactions via the (i) E-OH and (ii) S.A.-E reactions indicated by arrows. The E-OH and S.A.-E reactions can occur (a) intermolecularly to form crosslinks or (b) intramolecularly to form noncrosslinked internal rings, as illustrated in Fig. 22. Molecular modeling studies for low viscosity (η) cure conditions indicate ~75% of the E-OH and S.A.-E reaction occur by ring formation. (Higher η cure conditions would favor a higher percentage of ring formation.)

(v) Prepreg Processing Viscosity

To produce reproducible composites from prepregs, it is important for the prepreg to exhibit reproducible η-temperature-time profiles. Generally, prepregs are isothermally cured for a period of time at a

lower temperature (i.e., 130°C) prior to final cure at 177°C. A minimum in η will occur during this isothermal cure, and pressure is applied to the composite at this time to remove excess resin and to produce a void-free composite. The η of a liquid normally decreases with increasing temperature, but as the cure reactions occur the η will increase with increasing temperature and time. The magnitude and shape of the η-temperature-time profile of the prepreg will depend on (1) the initial η of MY720, (2) the temperature-time mixing conditions of the epoxy components and their introduction onto the C fibers and (3) the m.pt., catalytic activity and the distribution of the BF_3:amine catalyst within the prepreg. The size and distribution of the BF_3:amine catalyst particles within the prepreg is probably difficult to control and highly variable. Also, any recrystallization of the DDS in the prepreg changes the concentration of P.A. available for P.A.-E reactions below the DDS m.pt at 162°C. The rate of the P.A.-E cure reactions play the predominant role in the rate at which η increases with temperature and time.

D. PHYSICAL STRUCTURE

D.I. INTRODUCTION

The principal physical structural parameters that control the modes of deformation and failure and mechanical response of epoxies are (1) macroscopic inhomogenieties such as microvoids or concentrations of

unreacted monomer, (2) the glassy-state free volume and (3) the crosslinked network structure characteristics.

D.II. MACROSCOPIC INHOMOGENEITIES

Microvoids can result when air, moisture or other low molecular weight material is trapped in the system during cure and subsequently vaporized and possibly eliminated from the epoxy during postcure. The low molecular weight material results from either inhomogeneous mixing of the starting components or from aggregation, i.e. crystallization, of unreacted constituents. In polyamide-cured DGEBA epoxies, crystals of DGEBA epoxide monomer trapped in the partially cured resin at 23°C can produce microvoids by melting and volatilizing under certain post cure conditions.[71] Thermal-anneal, moisture-sorption and mechanical property studies also indicate that in TGDDM-DDS epoxies, the melting and volatilization of unreacted DDS crystallites during cure produces microvoids.[72]

D.III. FREE VOLUME

The mechanical properties of epoxies exhibit a free-volume dependence as a function of thermal history.[47,73,74] Changes in free volume, or local order, in the glassy state can occur as a result of the extension to temperatures below T_g of packing changes associated with the liquid state. The liquid-volume temperature plot extrapolated to below T_g in Fig. 23 represents the lower free-volume, equilibrium state of the

glass. The time necessary to achieve the equilibrium state at a given temperature below T_g depends on the glassy-state mobility. Below a specific temperature, the glassy-state mobility is too small to allow any changes in free volume. A decrease in free volume that occurs in the glassy state results in inhibition of the flow processes that occur during deformation and a more brittle mechanical response. Rapid cooling from above T_g, however, produces a glass with a larger free volume.

In addition to thermal history the free volume of epoxies also depends on the packing ability of the epoxide and amine structure and the geometric constraints imposed on the segmental packing by the crosslinked network geometry. Molecular model studies of DGEBA-T403 epoxies indicate that as the crosslink density of the network increases, the packing efficiency decreases. From compressibility studies, Findley and Reed[75] report lower crosslinked epoxies are more compact. Also, diffusion studies of H_2 and O_2 in crosslinked glasses indicate that the permeabilities will exhibit maxima at the highest crosslink density if the units that form the network inhibit close packing because of steric restrictions.[76-78] In our experimental studies on DGEBA-T403 epoxies we observed that these glasses exhibited a minimum in density and modulus and, therefore, maximum in free volume at the highest crosslink density. Furthermore, from dynamic mechanical measurements we observed the highest crosslink density DGEBA-T403 epoxy exhibited the largest secondary glass transition intensity. This observation implies the network segments responsible for the glassy state molecular motion associated with the secondary glass transition possess the greatest mobility and, therefore, free volume at the highest crosslink density.

D.IV. NETWORK STRUCTURE

The critical network structure parameters that control the mechanical performance of epoxies are macroscopic heterogeneities in crosslink density and the network topography on the molecular level.

Epoxies can form networks with heterogeneous crosslink density distributions in the 6 to 10,000 nm size range.[73,79-122] The formation of a heterogeneous rather than a homogeneous system depends on polymerization conditions, i.e. temperature, solvent, chemical composition and mixing of the starting materials. The high crosslink density regions have been described as agglomerates of colloidal particles[86,87] or floccules[91] in a lower molecular weight interstitial fluid. Funke[123,124] suggested a number of factors that can be responsible for heterogeneous network formation: 1) difference between the reactivities of different functional groups, 2) unreacted functional groups, 3) intramolecular cyclization reactions and 4) phase separation. Phase separation in the form of microgelation is generally believed to be the primary mechanism for the formation of heterogeneous crosslinked networks. Solomon et al.[90] originally suggested that a two-phase system is produced by mnicrogelation prior to the formation of a macrogel. Kenyon and Nielsen[94] indicated that the highly crosslinked microgel regions are loosely connected during the latter stages of the curing process. Karyakina et al.[104] suggested that microgel regions originate in the initial stages of polymerization from the formation of microregions of aggregates of primary polymer chains. Luettgert and Bonart[112] discussed the morphology of epoxies in terms of the relative

rates of microgel formation and the subsequent growth rate of these gel particles. At low cure temperatures, only a small number of gel particles are nucleated and, hence, large nonhomogeneities are produced; at higher cure temperatures, the rate of nucleation of microgel particles is faster, and larger numbers are produced, which, therefore, limits their growth in size. More recently, Bell[121] has postulated and shown that local regions of higher than average crosslink density can be attributed to inadequate mixing of the epoxy starting components. There have been no studies of the mutual solubilities of epoxy starting components as a function of temperature and composition.

The majority of the evidence for heterogeneous regions of crosslink density in epoxies is derived from electron microscope investigations. These microscopy studies involve carbon-platinum replication of etched and nonetched free surfaces and fracture surfaces. However, artifacts can often result from replication techniques.[26] More confidence can be placed in bright-field transmission electron microscopy studies of the morphology of thin epoxy films strained directly in the electron microscope.[110] The morphology of such thin films, however, may not be representative of the bulk. However, if the heterogeneous regions are sufficiently large as in the case of commercial TGDDM-DDS (25 wt% DDS, 0.4 wt% $BF_3:NH_2C_2H_5$) epoxies such regions can be detected directly by optical microscopy.[27,111]

Small angle x-ray scattering (SAXS) studies have the potential to monitor cross-linked network morphologies. Recent studies[125] conducted for us at the National Scattering Center, Oak Ridge did not detect any heterogeneous regions that could be associated with crosslink density variations in a number of epoxies utilized as high performance composite

matices. However, if such regions were detected by SAXS it would be necessary to understand the relationship between the density and degree of crosslinking of the network to interpret such observations. This requires an understanding of the network structure on the molecular level.

The network parameters that can affect the mechanical response of a crosslinked epoxy are the network defects and topography.

Network defects in the form of unreacted groups serve as sites for crack initiation and propagation. When such defects are non-randomly distributed within the network a nodular morphology will be observed upon fracture or chemical etching of the bulk network.

The ability of a crosslinked network to deform depends on the glassy-state free volume and network extensibility. The extensibility of the network segments rather than the molecular weight between crosslinks, M_c determines the ultimate network properties. From the theory of rubber elasticity, the maximum network extensibility is directly related to M_c by the expression, $\lambda_b \alpha M_c^{1/2}$[126]. In highly crosslinked systems, however, the extensibility of the network segments between crosslinks depends on specific rotational isomeric configurations of the segments and the perturbation of these configurations by geometric network constraints. The network topography of the highly crosslinked networks will also significantly affect the network extensibility. To describe the network topography of epoxies, we first of all investigate the basic ring structures of the network by molecular models. These studies indicate which ring structures are sterically possible. The ring structures for DGEBA-T403 epoxies are illustrated in Fig. 24. Molecular and computer modeling studies

indicate the deformability of these basic ring structures depends, 1) the extensibility of their sides; 2) the flexibility of their internal angles; and 3) their ability to undergo co-operative deformation with their interconnected neighbors. Their co-operative deformation is controlled by the regularity of the network topography which is determined by the different geometries of the basic rings and their orientation relative to one another. The more regular networks consist of interconnected rings of similar size and shape. However, the more irregular networks consist of rings with a variety of geometries that will develop overstrained segments at lower extensibilities. The fully crosslinked DGEBA-T403 epoxy network is relatively irregular as shown in Fig. 25. The deformability of the basic ring structures will also depend on the direction of the applied stress field relative to the ring structure. This orientation factor will significantly affect the networks that consist of regions of regularly oriented and interconnected rings.

The distribution in network segmental extensibilities controls failure initiation and propagation of the network. The segments with the lowest extensibilities at any given time in the failure process will carry a significant portion of the load and will undergo chain scission resulting in a process of progressive scission of the least extensible segments. Discrete rather than random distributions in the network extensibilities of epoxies exist because of the chemical nature of epoxy network formation.

E. DEFORMATION AND FAILURE MODES

Epoxies can undergo plastic flow prior-to or during failure if there is sufficient free volume and time for network segmental reorientation to occur. A variety of evidence shows that plastic flow can occur under tensile loads in crosslinked amine-cured epoxy glasses.[1,127] This flow can occur by homogeneous deformation, or inhomogeneously via crazing and/or shear banding. Cracks are often initiated in these glasses by a crazing process.

The tensile fracture topographies of un-notched amine-cured epoxies exhibit three characteristic regions: 1) a course initiation region; 2) a slow crack growth, smooth region; and 3) a fast crack growth, rough region.[1,71-73,110-127] The coarse initiation region, that can contain microvoids and/or fractured fibrils, is a result of crack propagation through coarse crazes and/or shear bands. The crack then imposes a higher stress field on the craze or flaw tip which produces a small plastic zone that results in a smooth fracture topography. Whether flow in this small plastic zone at the crack tip occurs by shear yielding or yielding under normal stresses is difficult to ascertain experimentally and will depend on the stress fields imposed on the epoxy immediately ahead of the crack tip. The area of the mirror fracture topography is a measure of the ability of the polymeric glass to undergo plastic flow at the propagating crack tip.

In Fig. 26, we schematically illustrate four stages of failure in epoxies under an increasing tensile load. In each stage we document the craze/crack structure, the stress at the craze/crack surface and the resultant fracture topography.

In addition to the fracture topography observations in the slower crack propagation regions of epoxies a number of additional observations also indicate permanent molecular flow can occur in amine-cured epoxy networks in the glassy state.

Amine-cured epoxies can exhibit macroscopic tensile yield stresses in the glassy state.[47,73] Such yield stresses exhibit similar free volume dependencies as a function of thermal history as non-crosslinked glasses such as polycarbonate.[47,73,128] From Eyring's theory of stress-activated viscous flow in polymers[129] the strain rate and temperature dependencies of the epoxy yield stresses produce activation volumes associated with chain segment jumps similar in magnitude to those volumes associated with flow in non-crosslinked glasses.[47] Furthermore, many of the amine-cured epoxies we have studied exhibit ultimate elongations in the 10-30% range in the glassy state.[1,47,72,73]

Transmission electron microscopy (TEM) and birefringence studies of strained and/or fractured epoxies have revealed more direct experimental evidence that molecular flow can occur in these glasses. Films of DGEBA-DETA (~11 wt% DETA) epoxies, ~1 µm thick, were strained directly in the electron microscope and the deformation processes were observed in bright-field TEM.[73,110] Coarse craze fibrils yielded inhomogeneously by a process that involved the movement of indeformable 6-9 nm diameter, highly crosslinked molecular domains past one another. The material between such domains yielded and became thinner as plastic flow occurred.

We have monitored the deformation processes of a number of amine-cured DGEBA epoxies under polarized light.[1,127] The most thorough study was conducted on DGEBA-T403 epoxies at 23°C as a function of strain level and epoxide:amine ratio. The birefringent patterns of a DGEBA-T403 stoichiometric epoxy (47 phr T403) as a function of strain are shown in Fig. 27. At strains $\lesssim 2.5\%$ only elastic deformations occur and homogeneous color changes produced under polarized light in this strain region disappear instantaneously upon removal of the load. In the 2.5-4% strain region, homogeneous elastic and plastic deformations occur, and upon removal of the load the homogeneous plastic deformation does not relax out, which results in a permanent homogeneous color change in the unstrained epoxy when viewed under polarized light. Above 4% strain, the plastic deformation becomes increasingly inhomogeneous with increasing strain as indicated by the development of birefringent fringes. Ultimately, a local region of high strain develops in the sample in the form of a diffuse shear band and a neck develops in this region. The orientation of the birefringent fringes are initially affected by the network defect topography but ultimately they orient as a shear band at $\approx 45°$ to the direction of the applied load. Fracture occurs in the high strain, shear band region. Occasionally, more than one diffuse shear band will develop in the sample.

For the off-stoichiometric DGEBA-T403 epoxies that are in the 30-75 phr T403 range, birefringent-strain studies indicate the following trends in the deformation processes for epoxies that increasingly are removed further from the stoichiometric T403 concentration: 1) plastic flow is initiated and also becomes inhomogeneous at lower strains; 2) the regions of high strain are less oriented and their associated shear

bands are less well developed upon crack propagation and ultimate failure through such regions. DGEBA-T403 epoxies in the 20-30 phr T403 range that exhibit ultimate elongations in the 20-70% range deform only in a homogeneous plastic fashion.

F. STRUCTURAL PARAMETERS THAT CONTROL MECHANICAL PROPERTIES

The flexibility and extensibility of a crosslinked epoxy network are determined by the available glassy-state free volume. If the free volume is insufficient to allow network segmental extensibility via rotational isomeric changes then the brittle mechanical response of the epoxy glass is not controlled by the network structure but rather by macroscopic defects such as microvoids. For epoxies with sufficient free volume that allows plastic network deformation the mechanical response is controlled by the network structure.

Studies on DGEBA-T403 epoxies[1] reveal the magnitudes of the yield stress, tensile strength (which is controlled by the flow properties of the epoxy) and Young's modulus are determined by the glassy-state packing and free volume. These mechanical properties follow the same trends as the density as a function of T403 concentration. The density of the DGEBA-T403 epoxies decreases with increasing T403 content with a slight minimum superimposed on such a downtrend at stoichiometry because of the constraints of the crosslinks on the network packing efficiency.

The ultimate extensibility of epoxy glasses depends on the network structure extensibility and its associated defects. We found the ultimate glassy-state extension for DGEBA-T403 epoxies is a maximum at

stoichiometry and decreases either side of stoichiometry as more defects are introduced into the network in the form of unreacted groups (Fig. 28). The presence of unreacted groups and their associated unconnected, non-load bearing segments results in higher loads being imposed under stress on those segments that are incorporated into the network. The higher segmental stresses enhance stress-induced chain scissions at lower network extensibilities. The critical concentration of chain scissions associated with crack initiation will be attained at increasingly lower network extensibilities as the initial concentration of unreacted groups in the network increases.

A non-random distribution of defects in the network, that produces the observed nodular morphologies in epoxies, results in weak paths in the network that favor crack propagation.

Impure starting materials will also cause network defects. We have found epoxies prepared from purified monomers with T_g's >130°C can exhibit excellent mechanical properties at 23°C with tensile strengths of ~140 MPa and ultimate elongations of 5-8%.[5]

The distribution of network segmental extensibilities controls crack initiation and propagation within the network. Embrittlement of the network can occur during plastic deformation as a result of network chain scission. There is experimental evidence that network chain scission does occur during the deformation of DGEBA-T403 epoxies. These epoxies have been strained up to 30% at 70°C and then the load removed and this strain completely annealed out at 100°C. The ductility of such epoxies decreased by 50% and their T_g's were lowered 8°C compared to reference specimens that were exposed to the same thermal history but were not stressed at 70°C. Such deterioration in the mechanical

response and T_g are consistent with network deterioration via chain scission. In more direct evidence (1) stress-FTIR studies of thin DGEBA-T403 epoxy films indicate permanent chemical changes occur after removal of the load after 10% strain at 23°C[5] and (2) Brown and Sandreczki[130] have detected free radicals by electron paramagnetic resonance studies after ballmilling these epoxies.

Hence, epoxies which possess networks free of defects with segments of equal extensibilities would be ideal tough glasses for composite matrices.

G. SERVICE ENVIRONMENT AGING

The durability of epoxy composite matrices in service environment depends on many complex interacting phenomena. The factors that control the critical path to ultimate failure or unacceptable damage depend specifically on the particular environmental conditions. These environmental factors include service stresses, humidity, temperature and solar radiation. The combined effects of thermal history, moisture exposure, and stress have a deleterious effect on the physical and mechanical integrity of epoxies. We have studied the effect of specific combinations of moisture, heat and stress on the physical structure, failure modes, and tensile mechanical properties of TGDDM-DDS epoxies.[131] Sorbed moisture polasticizers TGDDM-DDS epoxies and lowers their tensile strengths, ultimate elongations and moduli. The fracture topographies of the initiation cavity and mirror regions of these epoxies indicate that sorbed moisture enhances the craze initiation and

propagation processes. Fully cured epoxy networks with segments of equal extensibilities that are tough over a wide temperature range will exhibit good wet mechanical properties and will be less susceptible to stress-moisture aging.

One of the more extreme environmental conditions experienced by an epoxy composite matrix occurs during a suspersonic dash of a fighter aircraft. The aircraft dives from high altitudes (where outer surface temperature is -20 to -55°C) into a supersonic, low-altitude run during which aerodynamic heating raises the surface temperature to 100-150°C, in a matter of minutes. On reduction of speed, the outer surface temperature drops extremely rapidly at rates up to about 500°C/min. thus exposing the epoxy composite to a thermal spike. Simulation of such thermal spikes has been shown to increase the amount of moisture sorbed by the epoxy or epoxy composite.[132-138] However, after a certain number of consecutive thermal spikes, the amount of moisture sorbed ceases to increase. Browning[134,137] suggested that such increases result from microcracks caused by the moisture and temperature gradients present during the thermal spike. McKague[136] noted that damage does not occur unless the thermal-spike maximum temperature exceeds the T_g of the moist epoxy. In our studies we found that the amount of moisture sorbed by TGDDM-DDS epoxies was enhanced by about 1.6 wt% after exposure to a 150°C thermal spike.[131] No significant areas of microcracking were observed in the thermally spiked epoxies. We suggested the primary mechanism by which thermally spiked epoxies sorb additional moisture can be explained in terms of moisture-induced free volume changes.

H. REFERENCES

1. Morgan, R. J., Kong, F. M., and Walkup, C. M., Polymer 25, 375 (1984)

2. Morgan, R. J., Mones, E. T., Steele, W. J. and Deutscher, S. B., Proc. 12th National SAMPE Tech. Conf. p. 368-379 (1980).

3. Pruneda, C. O., Morgan, R. J., Kong, F. M., Hodson, J. A., Kershaw, R. P., and Casey, A. W., Proc. 29th National SAMPE Symp. p. 1213-1222 (1984).

4. Rinde, J.A., Chiu, I., Mones, E.T., and Newey, H. A., Composites Tech. Rev. 1 (2), 4 (1979).

5. Morgan, R. J., Walkup, C.M., Kong, F.M., and Mones, E.T., "Development of Epoxy Matrices for Filament-Wound Graphite Structures," Proc. 30th National SAMPE Symp. (In press); LLNL Report, UCRL-90946 (1984).

6. May, C. A., "Exploratory Development of Chemical Quality Assurance and Composition of Epoxy Formulations," Air Force Materials Laboratory Report, AFML-TR-76-112 (1976).

7. Carpenter, J. F., "Quality Control of Structural Non-Metallics," McDonnell Aircraft Report, Contract No. N00019-76-C-0138 (1977).

8. Trujillo, R. E. and Engler, B. P., "Chemical Characterization of Composite Prepreg Resins," Part 1, Sandia Laboratory Report, SAND 78-1504 (1978).

9. Mones, E. T. and Morgan, R. J., Polymer Preprints, ACS, 22, No. 2, 249 (1981).

10. Mones, E. T., Walkup, C. M., Happe, J. A. and Morgan, R. J., Proc. of 14th National SAMPE Tech. Conf. p. 89-100 (1982).

11. Morgan, R. J., Happe, J. A. and Mones, E. T., Proc. or 28th National SAMPE Symp. p. 596-607 (1983).

12. Wolf, C. J. and Grayson, M. A., McDonnell-Douglas Research Laboratories, Private Communication.

13. Pearce, P. J., Davidson, R. G. and Morris, C.E.M., J. Appl. Polym. Sci., 26, 2363 (1981).

14. Hagnauer, G. L. and Pearce, P. J., in "Epoxy Resin Chemistry, II," Editor R. S. Bauer, ACS Symp. Series, 221, Ch. 10, (1983).

15. Scola, D. A., Proc. of 15th National SAMPE Tech. Conf., p.9-20 (1983).

16. Morgan, R. J., Walkup, C. M. and Hoheisel, T. H., "Differential Scanning Calorimetry Studies of the Cure of Carbon Fiber-Epoxy Composite Prepregs," J. Appl. Polym. Sci. (In press).

17. Happe, J. A., Morgan, R. J. and Walkup, C.M., "^{1}H, ^{19}F and ^{11}B Nuclear Magnetic Resonance Characterization of BF_3:Amine Catalysts Used in the Cure of C Fiber-Epoxy Prepregs," Polymer (In press).

18. Harris, J. A. and Temin, S. C., J. Appl. Polym. Sci. 10, 523 (1966).

19. Landua, A. J., Polymer Preprints, ACS, 24 299 (1964).

20. Kaelble, D. H., in "Resins for Aerospace" ACS Symposium Series 132, Editor C. A. May, ACS, Washington, D.C., Ch. 29 (1980).

21. Cizmecioglu, M. and Gupta, A., SAMPE Quarterly, 13 No. 2, 16 (1982)

22. Gupta, A., Cizmecioglu, M., Coulter, D., Liang, R. H., Yavrouian, A., Tsay, F. D. and Moacanin, J., J. Appl. Polym. Sci., 27, 1011 (1983).

23. May, C. A., Dusi, M. R., Fritzen, J.S., Hadad, D. K., Maximovich, M. G. and Thrasher, K. S., Organic Coat and Appl. Polym. Sci. Proc. 47, 419 (1982).

24. Lee, H. and Neville, K., "Handbook of Epoxy Resins," McGraw-Hill, New York (1967).

25. Sanjana, Z. M., Schaefer, W. H., and Ray, J. R., Polym. Eng. and Sci. 21, 474 (1981).

26. Morgan, R. J., in "The Role of the Polymeric Matrix in Processing and Structural Properties of Composite Materials," Editors J. Saferis and G. Nicolais, Plenum Press, p. 207-214 (1983).

27. Morgan, R. J. and Mones, E. T., "The Cure Reactions, Network Structure and Mechanical Response of Diaminodiphenyl Sulfone Cured Tetraglycidyl 4,4'Diaminodiphenyl Methane Epoxies," Polymer (submitted).

28. Narracott, E., Brit. Plast., 26, 120 (1953).

29. Shechter, L., Synstra, J., and Kurkjy, R. P., Ind. Eng. Chem., 48, 94 (1956).

30. Simons, D. M. and Verbanc, J.J., J. Polym. Sci., 44, 303 (1960).

31. Anderson, H. C., SPE Journal, 16, 1241 (1960).

32. Kakurai, T. and Noguchi, T., J. Soc. Org. Syn. Chem. Japan, 18, 485 (1960).

33. Smith, I. T., Polymer, $\underline{2}$, 95 (1961).

34. Kwei, T. K., J. Polym. Sci., $\underline{1A}$, 2985 (1963).

35. Stille, J. K., and Culbertson, B. M., J. Polym. Sci., $\underline{A,2}$, 405 (1964).

36. Lee, L. H., J. Polym. Sci., $\underline{A,3}$, 859 (1965).

37. Price, C. C. and Carmelite, D. D., J. Am. Chem. Soc., $\underline{88}$, 4039 (1966).

38. Lee, H. and Neville, K., "Handbook of Epoxy Resins," McGraw-Hill, New York, 1967.

39. Bauer, R. S., J. Polym. Sci., $\underline{A-1}$, 5, 2192 (1967).

40. Sorokin, M. F., Shode, L. G. and Steinpress, A. B., Vysokomol. Soyed, $\underline{A14}$, 309 (1972).

41. Sorokin, M. F., Shode, L. G., Drobrovinskii, L. A., and Onosov, G. V., Vysokomol, Soyed, $\underline{A14}$, 2420 (1972).

42. Sidyakin, P. V., Vyskomol. Soyed., $\underline{A14}$, 979 (1972).

43. Tanaka, Y. and Mika, T. F. in "Epoxy Resins Chemistry and Technology, " Eds. May, C. A. and Tanaka, Y., Dekker, New York, Ch.3, 1973.

44. Whiting, D. A. and Kline, D. E., J. Appl. Polym. Sci., $\underline{18}$, 1043 (1974).

45. Dusek, K. and Bleha, M., J. Polym. Sci. (Polym. Chem. Ed.), $\underline{15}$, 2393 (1977).

46. Schneider, N. S., Sprouse, J. F., Hagnauer, G. L. and Gillham, J. K., Polym. Eng. and Sci., $\underline{19}$, 304 (1979).

47. Morgan, R. J., J. Appl. Polym. Sci., $\underline{23}$, 2711 (1979).

48. Bokare, U.M. and Gandhi, K.S., J. Polym. Sci. (Polym. Chem. Ed.), $\underline{18}$, 857 (1980).

49. Stevens, G. C., J. Appl. Polym. Sci., $\underline{26}$, 4259 (1981).

50. Allen, F. J. and Hunter, W. M., J. Appl. Chem., $\underline{7}$, 86 (1957).

51. Fowler, G. W. and Fitzpatrick, J. T., U.S. Patent 2,426,264, 1947.

52. Haynes, L. T., Heilbron, I., Jones, E.R.H. and Sondheimer, F., J. Chem. Soc., 1583 (1947).

53. Fife, H. F. and Roberts, F. H., Brit. Patent, 601,608, (1948).

54. Letsinger, R. L., Traynham, J. G. and Bobko, E., J. Am. Chem. Soc., 74, 399 (1952).

55. Jacobs, T. L., Dankner, D. and Dankner, H. R., J. Am. Chem. Soc., 80, 864 (1958).

56. Burness, D. M., J. Org. Chem., 29, 1862 (1964).

57. Bell, J. P. and McCarvill, W. T., J. Appl. Polym. Sci., 18, 2243, (1974).

58. Keenan, M. A. and Smith, D. A., J. Appl. Polym. Sci., 11, 1009, (1967).

59. Paterson-Jones, J. C. and Smith, D. A., J. Appl. Polym. Sci., 12, 1601 (1968).

60. Bishop, D. P. and Smith, D. A., J. Appl. Polym. Sci., 14, 205 (1970).

61. Leisegang, E. C., Stephen, A. M. and Paterson-Jones, J. C., J. Appl. Polym. Sci., 14, 1961 (1970).

62. Paterson-Jones, J. C., J. Appl. Polym. Sci., 19, 1539 (1975).

63. Butler, G. B., Polymer Preprints, ACS, 8, 35 (1967).

64. Moacanin, J., Cizmecioglu, M., Tsay, F. and Gupta, A., Org. Coat. and Appl. Polym. Sci. Preprints, ACS, 47, 587 (1982).

65. General Dynamics Report F33615-80-C-5021 (1980).

66. Bell, J. P., J. Polym. Sci. A-2, 417 (1970).

67. Mijovic, J., Kim, J. and Slaby, J., J. Appl. Polym. Sci., 29, 1449, (1984).

68. Grayson, M. A. and Wolf, C. J., J. Polym. Sci. (Polymer Physics Edition) (In press).

69. Wolf, C. J. McDonnell-Douglas Research Laboratories, Private Communication.

70. David C., in Comprehensive Chemical Kinetics, Vol. 14, Degradation of Polymers, Ed. Bamford, C. H. and Typer, C.F.H., Elsevier, p.1. (1975).

71. Morgan, R. J. and O'Neal, J. E., J. Macromol. Sci. Phys., B15 (1), 139 (1978).

72. Morgan, R. J., O'Neal, J. E. and Miller, D. B., J. Materials Sci. 14, 109 (1979).

73. Morgan, R. J., and O'Neal, J. E., Polym. Plast. Technology, 10(1), 49 (1978).

74. Kong, E. S., Wilkes, G. L., McGrath, J. E., Banthia, A. K. Mohajer, Y;, and Tant, M. R., Polym. Eng. and Sci., 21, 943 (1981).

75. Findley, W. N. and Reed, R. M., Polym. Eng. Sci. 27, 837 (1977).

76. Barton, J. M. Polymer 20, 1018 (1979).

77. Gordon, G. A. and Ravve, A., Polym. Eng. Sci. 20, 70 (1980).

78. Diamant, Y., Marom, G., and Broutman, L. J., J. Appl. Polym. Sci., 26, 3015 (1981).

79. Carswell, T. S., Phenolplasts, Interscience, New York (1947).

80. Rochow, T. G. and Rowe, F. G. Anal. Chem., 21, 261 (1949).

81. Spurr, R. A., Erath, E. H., Myers, H. and Pease, D. C. Ind. Eng. Chem. 49, 1839 (1957).

82. Spurr, R. A., Erath, E. H., Myers, H. and Pease, D. C. Ind. Eng. Chem. 49, 1839 (1957).

83. Erath, E. H. and Spurr, R. A., J. Polym. Sci. 35, 391 (1959).

84. Rochow, T. G. Anal. Chem. 33, 1810 (1961).

85. Gallacher, L. and Bettelheim, F. A., J. Polym. Sci. 59, 697 (1962).

86. Erath, E. H. and Robinson, J., J. Polym. Sci. Part C, 3, 65 (1963).

87. Wohnsiedler, H. P., J. Polym. Sci., Part C, 3, 77 (1963).

88. Lewis, A. F., SPE Trans, 3, 201 (1963).

89. Lewis, A. F. and Ramsey, W. B., Adhes. Age, 9, 20 (1966).

90. Solomon, D. H., Loft, B. C. and Swift, J. D., J. Appl. Polym. Sci., 11, 1593 (1967).

91. Cuthrell, R. E., J. Appl. Polym. Sci. 11, 949 (1967).

92. Neverov, A.N., Birkina, N. A., Zherdev,. Yu, V. and Kozlov, V. A., Vysokomol. Soedin, A10, 463 (1968).

93. Nenkov, G. and Mikhailov, M. Makromol. Chem. 129, 137 (1969).

94. Kenyon, A. S. and Nielsen, L. E., J. Macromol. Sci. Chem. A3(2), 275 (1969).

95. Strecker, R.A.H., J. Appl. Polym. Sci. 13, 2439 (1969).

96. French, D. M., Strecker, R.A.H., and Tompa, A.S., J. Appl. Polym. Sci., 14, 599 (1970).

97. Turner, D. T. and Nelson, B. E., J. Polym. Sci. Polym. Phys. Ed., 10, 2461 (1972).

98. Basin, V. YE., Korunskii, L.M., Shokalskaya, O.Y. and Aleksandrov, N. V., Polym. Sci. USSR, 14, 2339 (1972).

99. Kessenikh, R. M., Korshunova, L.A. and Petrov, A.V., Polym. Sci., USSR, 14, 466 (1972).

100. Bozveliev, L. G. and Mihajlov, M. G., J. Appl. Polym. Sci., 17, 1963 (1973); J. Appl. Polym. Sci., 17, 1973 (1973).

101. Kreibich, U. T. and Schmid, R., J. Polym. Sci. Symp. 53, 177 (1975).

102. Morgan, R. J. and O'Neal, J. E. Polym., Preprints, ACS, 16 (2), 610 (1975).

103. Selby, K. and Miller, L. E., J. Mater. Sci. 10, 12 (1975).

104. Karyakina, M.I., Mogilevich, M. M., Maiorova, N.V. and Udalova, A.V., Vysokomol. Soedin, A17, 466 (1975).

105. Maiorova, M.V., Mogilevich, M. M., Karyakina, M.I. and Udalova, A.V., Vysokomol. Soedin, A17, 471 (1975).

106. Smartsev, V.M., Chalykh, A. YE., Nenakhov, S.A. and Sanzharovskii, A. T. Vysokomol. Soedin, A17, 836 (1975).

107. Morgan, R. J. and O'Neal, J. E., Polym. Plast. Technol. Eng. 5 (2), 173 (1975).

108. Racich, J. L. and Koutsky, J.A., J. Appl. Polym. Sci., 20, 2111 (1976).

109. Morgan, R. J. and O'Neal, J. E. in Toughness and Brittleness of Plastics, Advances in Chemistry Series 154, Eds. R. D. Deanin and A. M. Grugnola, (ACS, Washington, D.C.), Ch. 2 (1976).

110. Morgan, R. J. and O'Neal, J. E., J. Mater. Sci. 12, 1966 (1977).

111. Morgan, R. J. and O'Neal, J. E. in Chemistry and Properties of Crosslinked Polymers, Ed., S. S. Labana, Academic Press, p. 289-301 (1977).

112. Luettgert, K.E. and Bonart, R. Prog. Colloid. Polym. Sci. 64, 38 (1978).

113. Dusek, K., Plestil, J., Lednicky, F. and Lunak, S., Polymer 19, 393 (1978).

114. Schmid, R., Prog. Colloid. Polym. Sci. 64, 17 (1978).

115. Mijovic, J.S. and Koutsky, J. A., Polymer 20, 1095 (1979).

116. Mijovic, J.S. and Koutsky, J.A., J. Appl. Polym. Sci. 23, 1037 (1979).

117. Aspbury, P. J. and Wake, W. C., Br. Polym. J. 11, 17 (1979).

118. Matyi, R. J., Uhlmann, D. R. and Koutsky, J.A., J. Polym. Sci., Polym. Phys. Ed. 18, 1053 (1980).

119. Mijovic, J. and Tsay, L., Polymer 22, 902 (1981).

120. Oberlin, A., Ayache, J., Oberlin, M. and Guigon, M., J. Polym. Sci. (Polymer Phys. Ed.) 20, 579 (1982).

121. Bell, J.P., Org. Coatings & Appl. Polym. Sci. 46, 585 (1982).

122. Takahama, T. and Geil, P.H., Makromol. Chem., Rapid Commun. 3, 389 (1982).

123. Funke, W. Chimia, 22, 111 (1968).

124. Funke, W., Beer, W. and Seitz, U., Prog. Colloid. Polym. Sci. 57, 48 (1975).

125. Fellers, J. F. and Lee, J.S., SAXS Studies of Polymeric Materials Used in High Performance Composites, Lawrence Livermore National Laboratory Progress Report, P.O. 281901 August (1983).

126. Kaelbe, D.H., in Epoxy Resins, Chemistry and Technology, C. A. May and Y. Tanaka, Eds., Marcel Dekker, New York, Ch. 5 (1973).

127. Morgan, R. J., Mones, E. T. and Steele, W. J., Polymer 23, 295 (1982).

128. Morgan, R. J. and O'Neal, J. E., J. Polym. Sci., Polymer Phys. Ed., 14, 1053 (1976).

129. Eyring, H., J. Chem. Phys. 4, 283 (1936).

130. Brown, I. M. and Sandreczki, T. C., McDonnell Douglas Research Laboratories, St. Louis, personal communication.

131. Morgan, R. J., O'Neal, J. E. and Fanter, D. L., J. Materials Sci. 15, 751 (1980).

132. Verette, R. M., Temperature/humidity effects on the strength of graphite epoxy laminates, AIAA Paper No. 75-1011 (1975).

133. McKague, E. L.,Jr., Halkias, J. E. and Reynolds, J.D.J. Compos. Mater. 9, 2 (1975).

134. Browning, C. E., Ph.D. thesis, University of Dayton, Dayton, Ohio 1976.

135. Hedrick, I.G. and Whiteside, J.B., Effects of Environment on Advanced Composite Structures in AIAA Conference on aircraft composites: the emerging methodology of structural assurance, San Diego, CA, Paper No. 77-463 (1977).

136. McKague, E. L. Chapter 5 in Proceedings of Conference on Environmental Degradation of Engineering Materials', eds Louthan, M. R. and McNitt, R.P., Virginia Polytechnic Inst. Printing Dept., Blacksburg, VA p. 353 (1977).

137. Browning, C. E., The mechanism of elevated temperature property losses in high performance structural epoxy resin matrix materials after exposure to high humidity environments, 22nd National SAMPE Symposium and Exhibition, San Diego, CA 22, 365 (1977).

138. Advanced Composite Materials--Environmental Effects, ASTM STP 658, ed. Vinson, J.P., American Society for Testing and Materials, Phila. PA (1978).

FIGURE CAPTIONS

Fig. 1   Chemical structure of DGEBA epoxide and T403 polyethertriamine curing agent.

Fig. 2   Epoxide consumption vs. T403 amine concentration for DGEBA-T403 epoxies cured at 85°C, 24h.

Fig. 3   The structure of TGDDM and DDS monomers.

Fig. 4 ^{1}H NMR spectra of commercial $BF_3:NH_2C_2H_5$ samples (A = Harshaw, B = Alfa, C = K, and K, D = Pfaltz and Bauer); (a) and (b) illustrate two different CH_2 components.

Fig. 5 ^{19}F NMR spectra of commercial $BF_3:NH_2C_2H_5$ samples (A = Harshaw, B = Alfa, C = K, and K, D = Pfaltz and Bauer).

Fig. 6 ^{19}F NMR spectrum of DMSO-extracted components from Fiberite 934 prepreg.

Fig. 7   DSC plots for TGDDM (64 wt%)/DDS (25%)/DGOP (11 wt%) epoxy prepreg mixture with (a) 0.0 wt% and (b) 0.4 wt% $BF_3:NH_2C_2H_5$ catalyst.

Fig. 8   DSC ΔH peak intensities in j/g versus the temperature associated with maximum peak intensity for 1, 2, 3 and 4 component mixtures of TGDDM/DDS/DGOP/$BF_3:NH_2C_2H_5$ epoxies and commercial Fiberite 934 prepreg.

Fig. 9 ΔH values for the DSC α, β and γ peaks in TGDDM (64 wt%)/DDS (25 wt%)/DGOP (11 wt%) epoxies as a function of $BF_3:NH_2C_2H_5$ concentration.

Fig. 10   % of unreacted epoxide groups vs cure conditions for pure TGDDM ($\square$), MY720 ($\triangle$), MY720 + 0.4 wt% $BF_3:NH_2C_2H_5$ -non-acetone mixed ($\diamondsuit$), MY720 + 0.4 wt% $BF_3:NH_2C_2H_5$-acetone mixed ($\bigcirc$).

Fig. 11   Hydroxyl group IR intensity (A_{3500}/A_{1615}) vs cure conditions for pure TGDDM ($\square$), MY720 ($\triangle$), MY720 + 0.4 wt% $BF_3:NH_2C_2H_5$-non-acetone mixed ($\diamondsuit$), MY720 + 0.4 wt% $BF_3:NH_2C_2H_5$-acetone mixed ($\bigcirc$).

Fig. 12   Ether group IR intensity (A_{1120}/A_{805}) vs cure conditions for pure TGDDM ($\square$), MY720 ($\triangle$), MY720 + 0.4 wt% $BF_3:NH_2C_2H_5$ non-acetone mixed ($\diamondsuit$), MY720 + 0.4 wt% $BF_3:NH_2C_2H_5$-acetone mixed ($\bigcirc$).

Fig. 13   Carbonyl Group IR Intensity (A_{1720}/A_{805}) vs cure conditions for pure TGDDM ($\square$), MY720 ($\triangle$), MY720 + 0.4 wt% $BF_3:NH_2C_2H_5$-non-acetone mixed ($\bigcirc$).

Fig. 14   Epoxides ($\bullet$) and P.A.'s ($\blacktriangle$) (% of unreacted groups), R_{OH}($\blacksquare$) R_{ether}) ($\blacklozenge$) $I_{NH:SO_2}$(X) vs cure time at 177°C for TGDDM-DDS

(25 wt% DDS) (0.4 wt% $BF_3:NH_2C_2H_5$) epoxy.

Fig. 15   % of unreacted epoxide and P.A. groups, $I_{NH:SO_2}$, R_{ether} and R_{OH} values vs cure conditions in the 177-300°C range and DDS concentration for TGDDM-DDS (0 wt% $BF_3:NH_2C_2H_5$) epoxies.

Fig. 16   % of epoxide groups consumed at 177°C after 2.5 hrs vs wt% DDS for (i) TGDDM-DDS (0 wt% $BF_3:NH_2C_2H_5$)(———); (ii) TGDDM-DDS (0.4 wt% $BF_3:NH_2C_2H_5$) non-acetone mixed (----); (iii) TGDDM-DDS (0.4 wt% $BF_3:NH_2C_2H_5$) acetone mixed (-·-·-·); (iv) 100% completed P.A.-E reaction (......) and (v) 50% completed S.A.-E reaction (-··-··-).

Fig. 17 $I_{NH:SO_2}$ intensity after 2.5 hrs at 177°C vs DDS concentration for TGDDM-DDS epoxies.

Fig. 18 R_{OH} values after 177°C-2.5 hr cure vs DDS concentration for TGDDM-DDS epoxies.

Fig. 19   (a) R_{ether} values after 177°C-2.5 hr cure vs DDS concentration and (b) R_{ether} values vs cure temperature for TGDDM-DDS epoxies.

Fig. 20   % epoxide consumed by each cure reaction vs total % epoxide consumed.

Fig. 21   Primary amine-epoxide reaction ((i) and (ii) - sites for E-OH and SA-E reactions respectively.)

Fig. 22   (i) Epoxide-hydroxyl and (ii) secondary amine-epoxide reactions that form (a) intermolecular crosslinks and (b) intramolecular rings.

Fig. 23   Volume-temperature plot for a polymer.

Fig. 24   Ring structures in DGEBA-T403 epoxy networks.

Fig. 25   Network structure of fully reacted stoichiometric DGEBA-T403 epoxy.

Fig. 26   Microscopic failure processes in epoxies in tension.

Fig. 27   Birefringent deformation processes in DGEBA-T403 (47 phr T403) epoxy as a function of strain at 23°C, under polarized light.

Fig. 28   The ultimate tensile strain vs T403 concentration for DGEBA-T403 epoxies, at 23°C.

$$CH_2-CH-CH_2-O-\langle O \rangle - \underset{\underset{CH_3}{|}}{\overset{\overset{CH_3}{|}}{C}} - \langle O \rangle - O - CH_2 - CH - CH_2$$
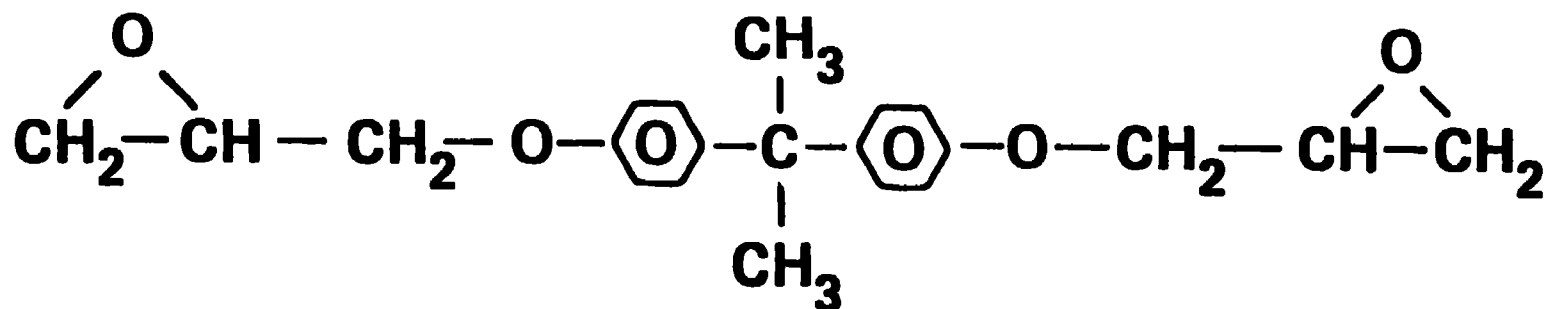
**Diglycidyl ether of bisphenol A
(DOW DER 332)**

$$H_2C -[O\ CH_2\ CH\ (CH_3)]_x\ NH_2$$

$$CH_3CH_2\underset{|}{\overset{|}{C}}CH_2 -[O\ CH_2\ CH\ (CH_3)]_y\ NH_2$$

$$H_2C -[O\ CH_2\ CH\ (CH_3)]_z\ NH_2$$

$$x + y + z \simeq 5.3$$
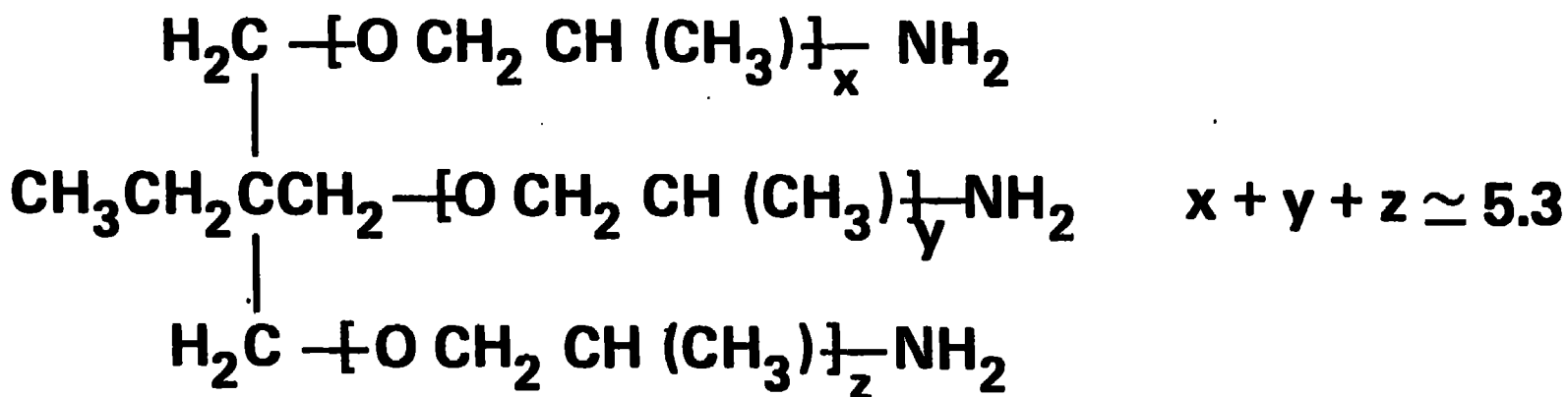
**Polyether triamine
(Jefferson T403)**

FIGURE 1
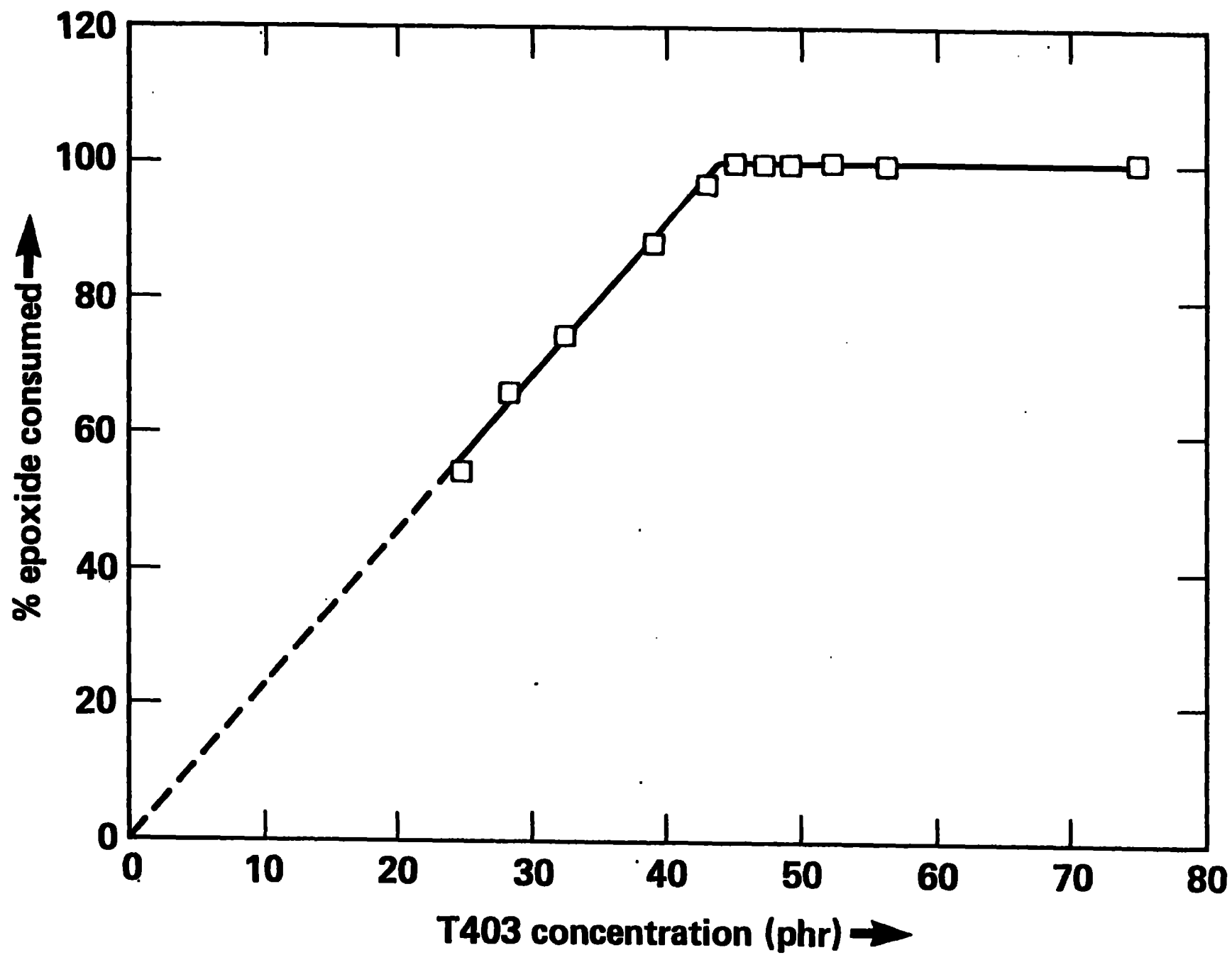
FIGURE 2
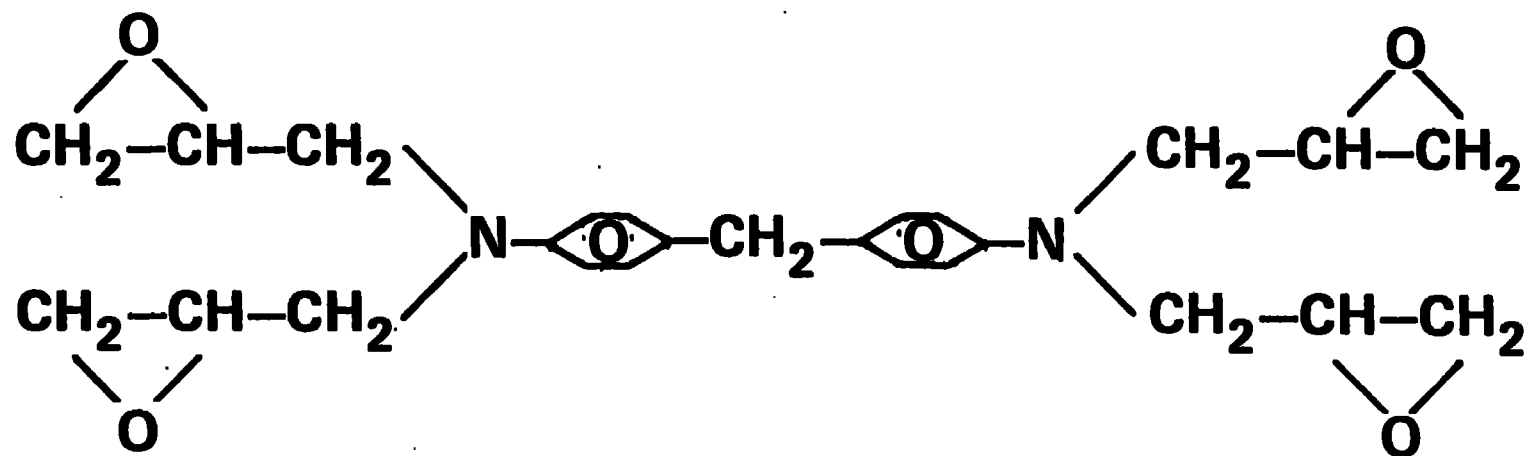
Tetraglycidyl 4, 4′ diaminodiphenyl methane epoxy TGDDM (liquid at 23°C)
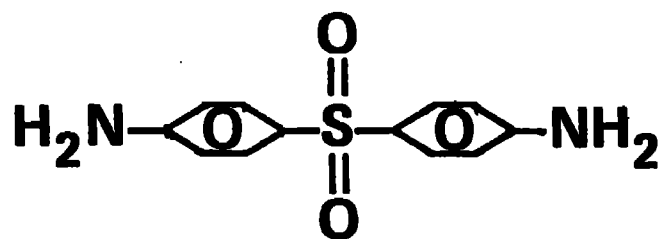
4, 4′ diaminodiphenyl sulfone DDS (crystalline solid, mp 162°C)

FIGURE 3
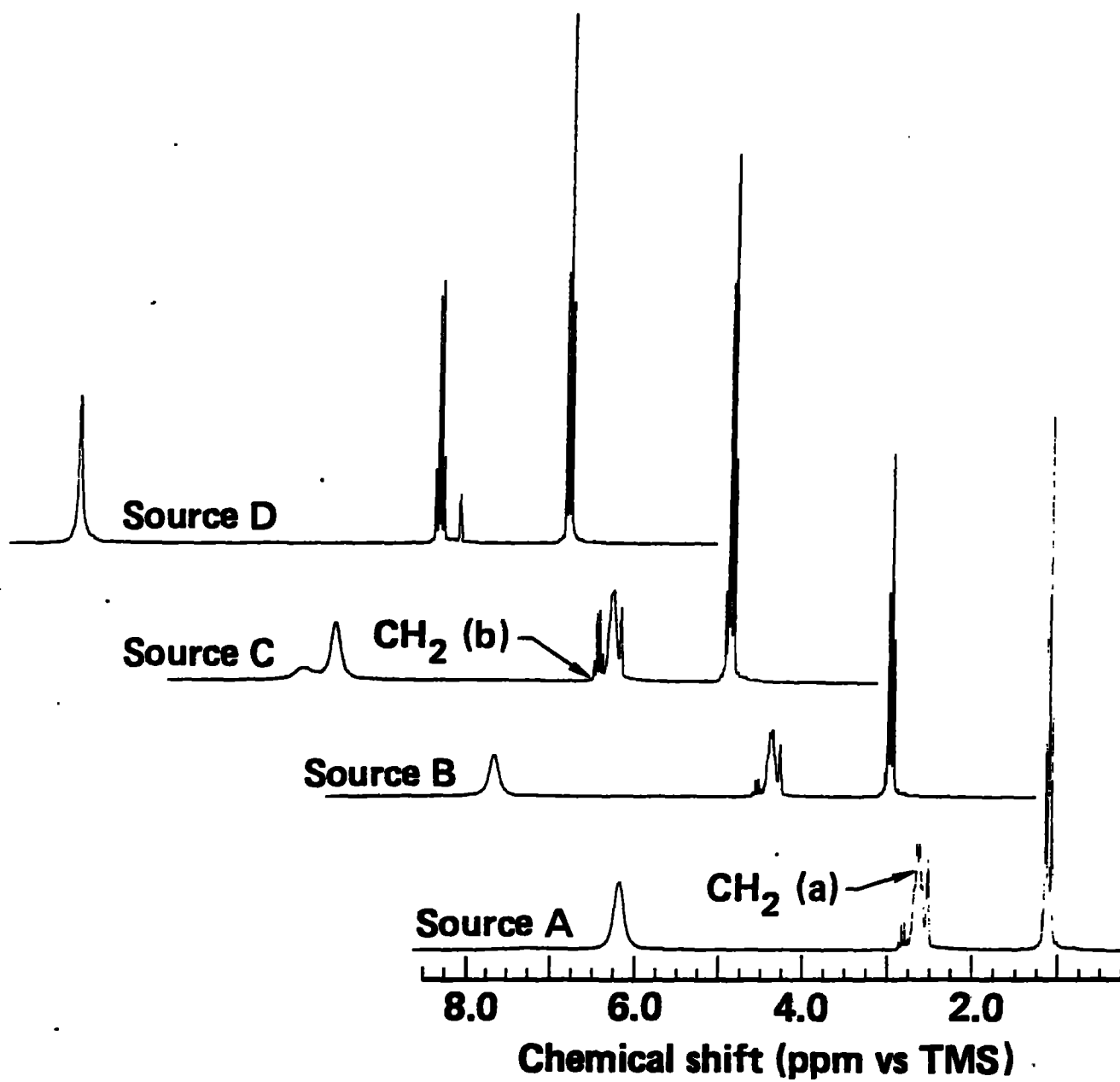
FIGURE 4
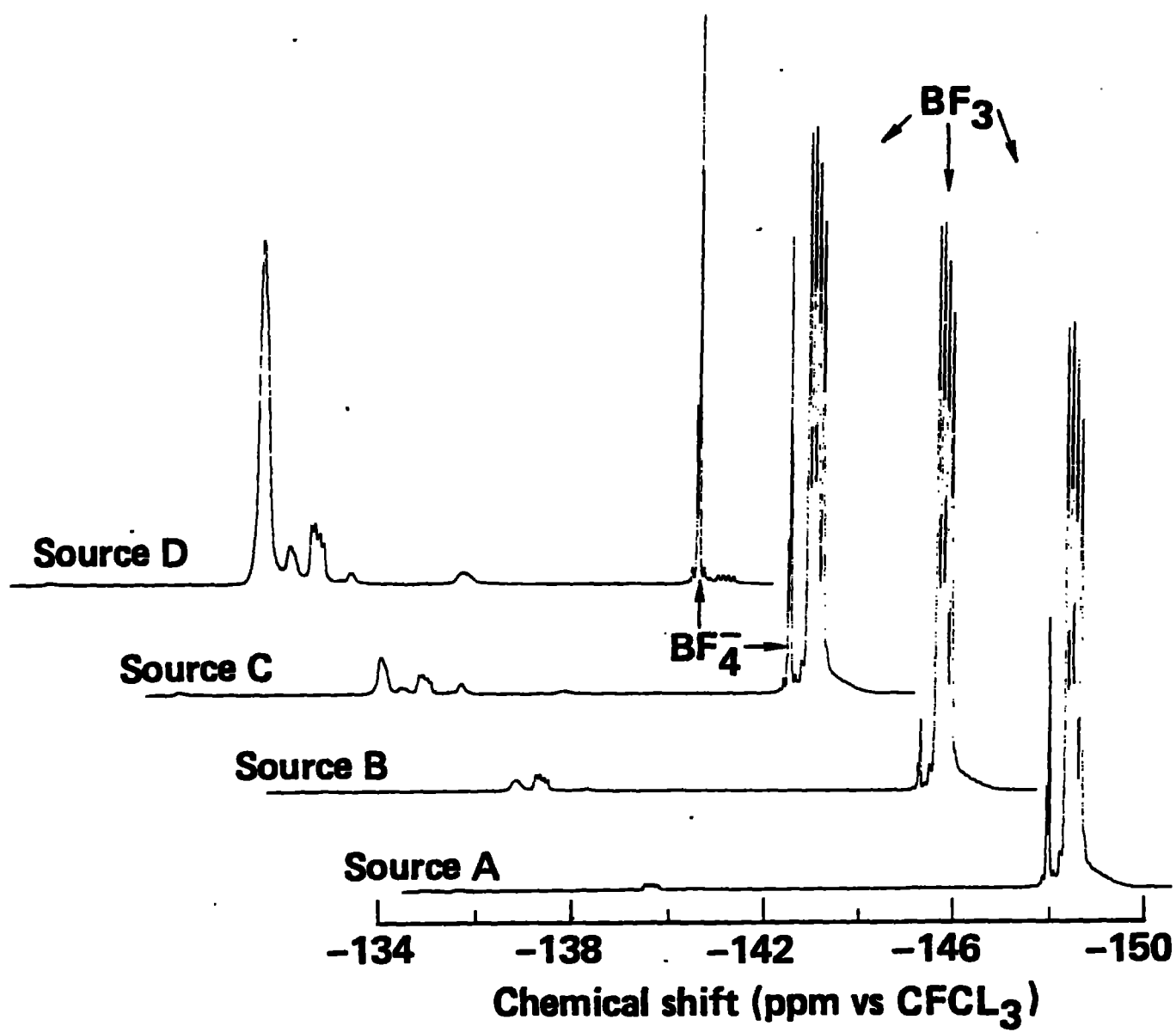
FIGURE 5
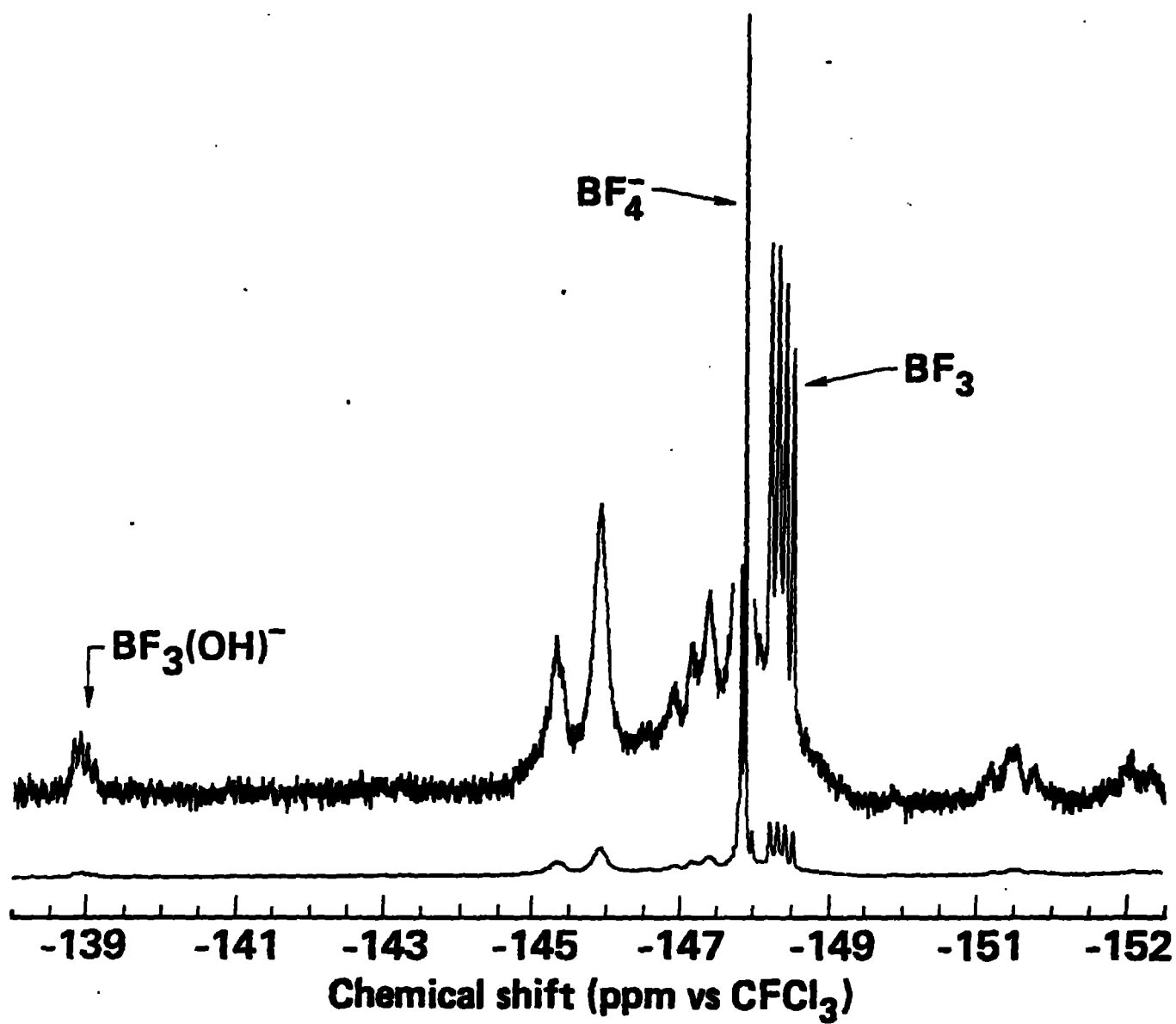
FIGURE 6
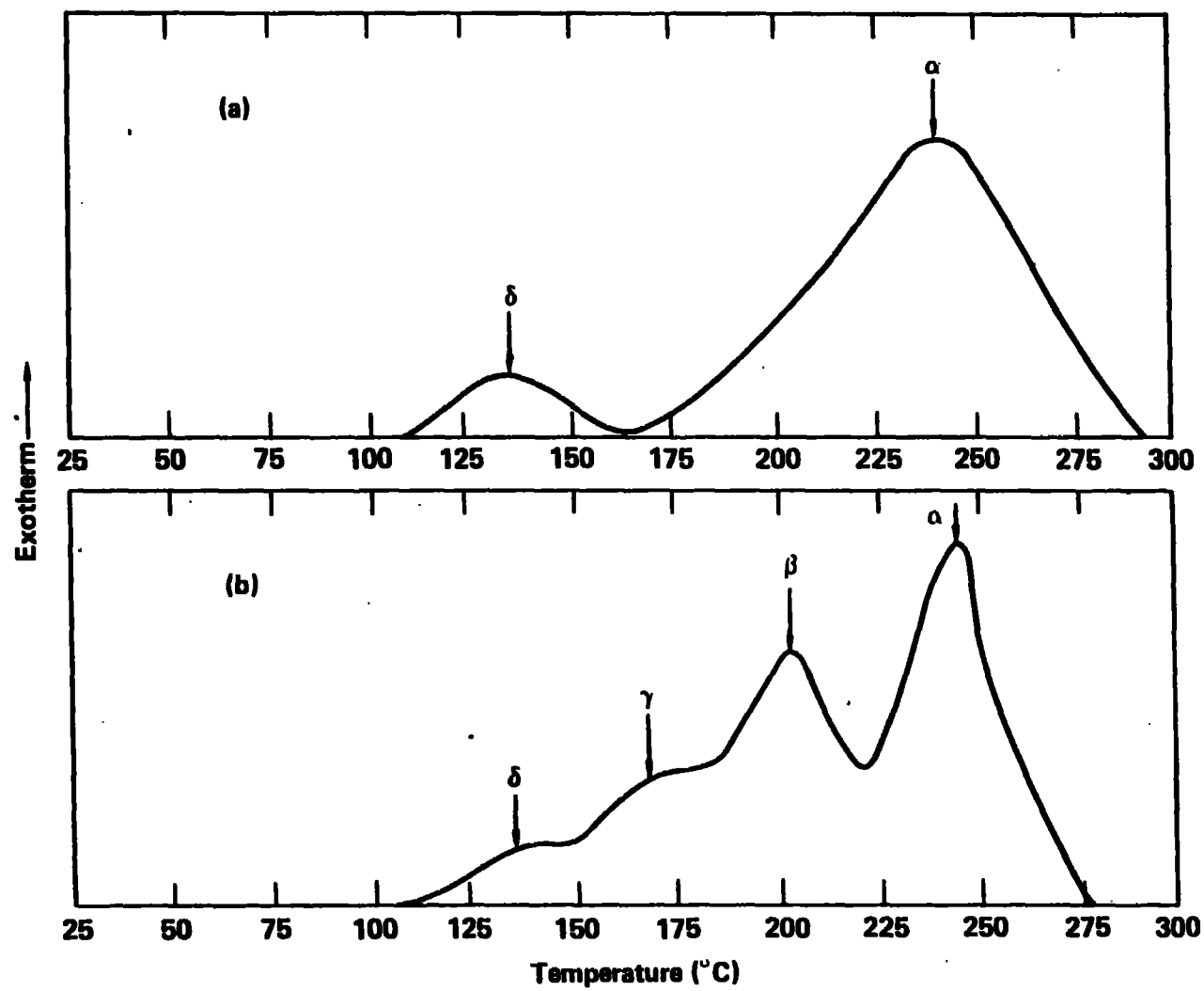
FIGURE 7

FIGURE 8

FIGURE 9

% unreacted epoxide groups

Legend:
- □ Pure TGDDM
- △ MY720
- ○ MY720 + BF$_3$:NH$_2$C$_2$H$_5$ acetone mixed
- ◇ MY720 + BF$_3$:NH$_2$C$_2$H$_5$ non acetone mixed

Temperature °C
Time (hours)
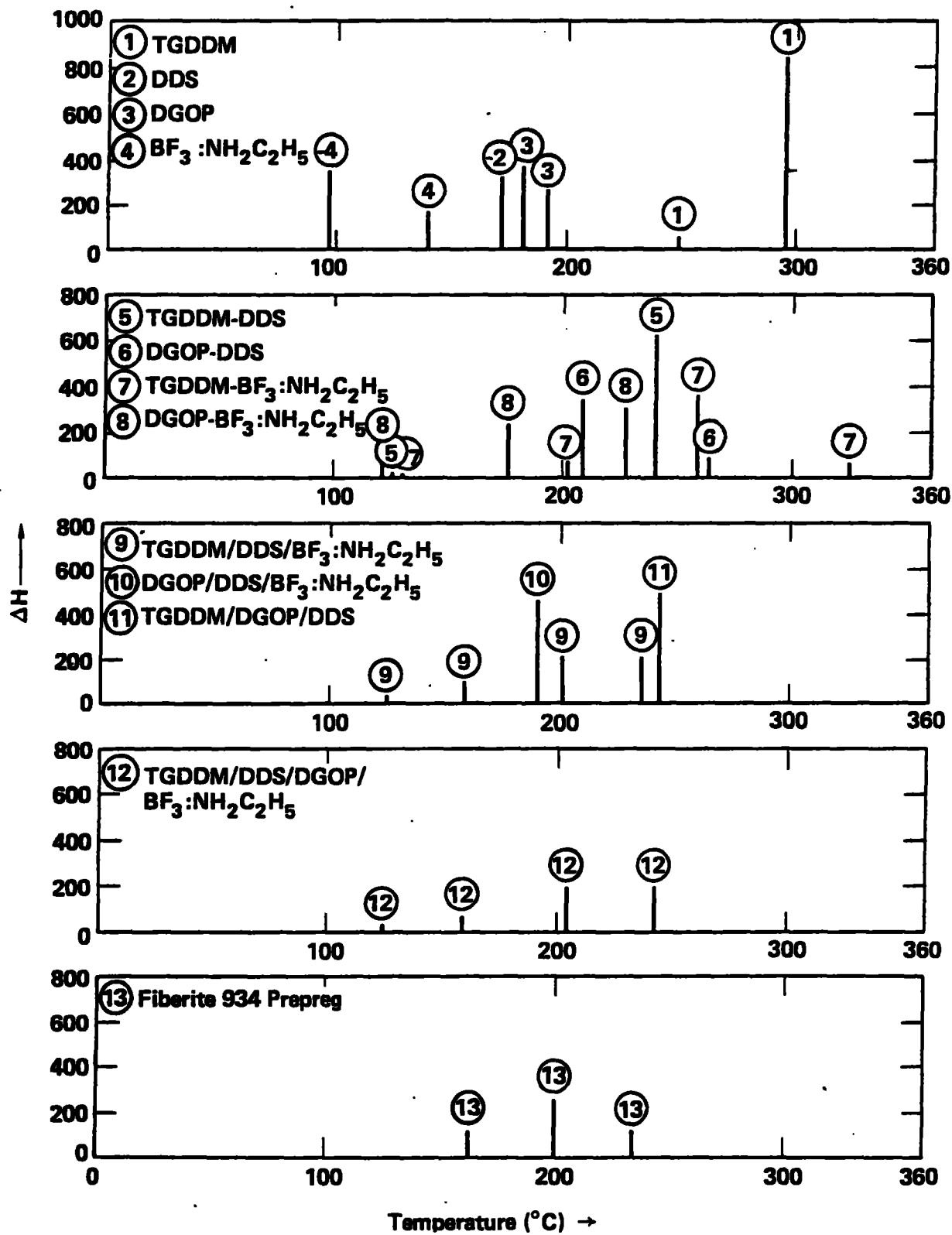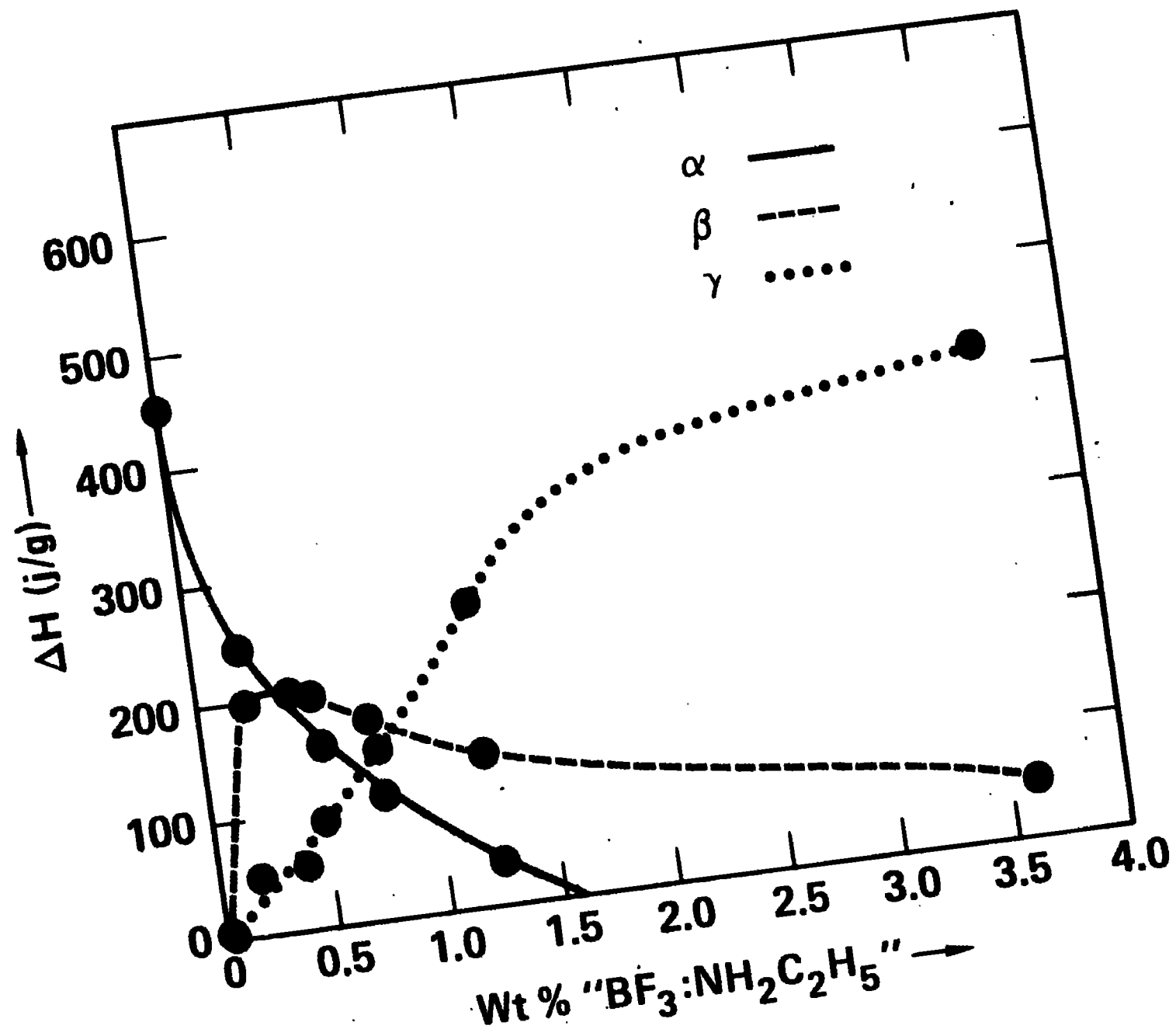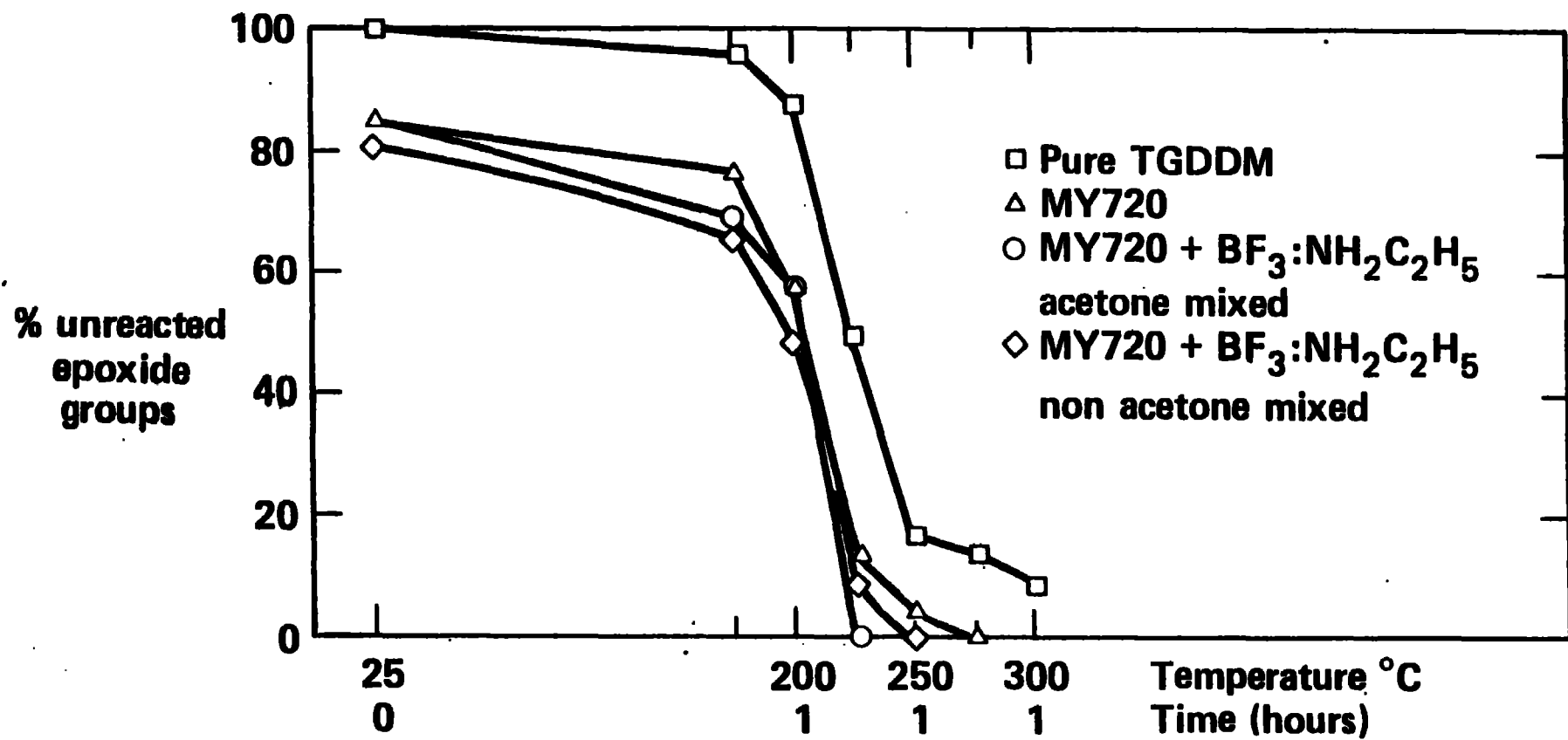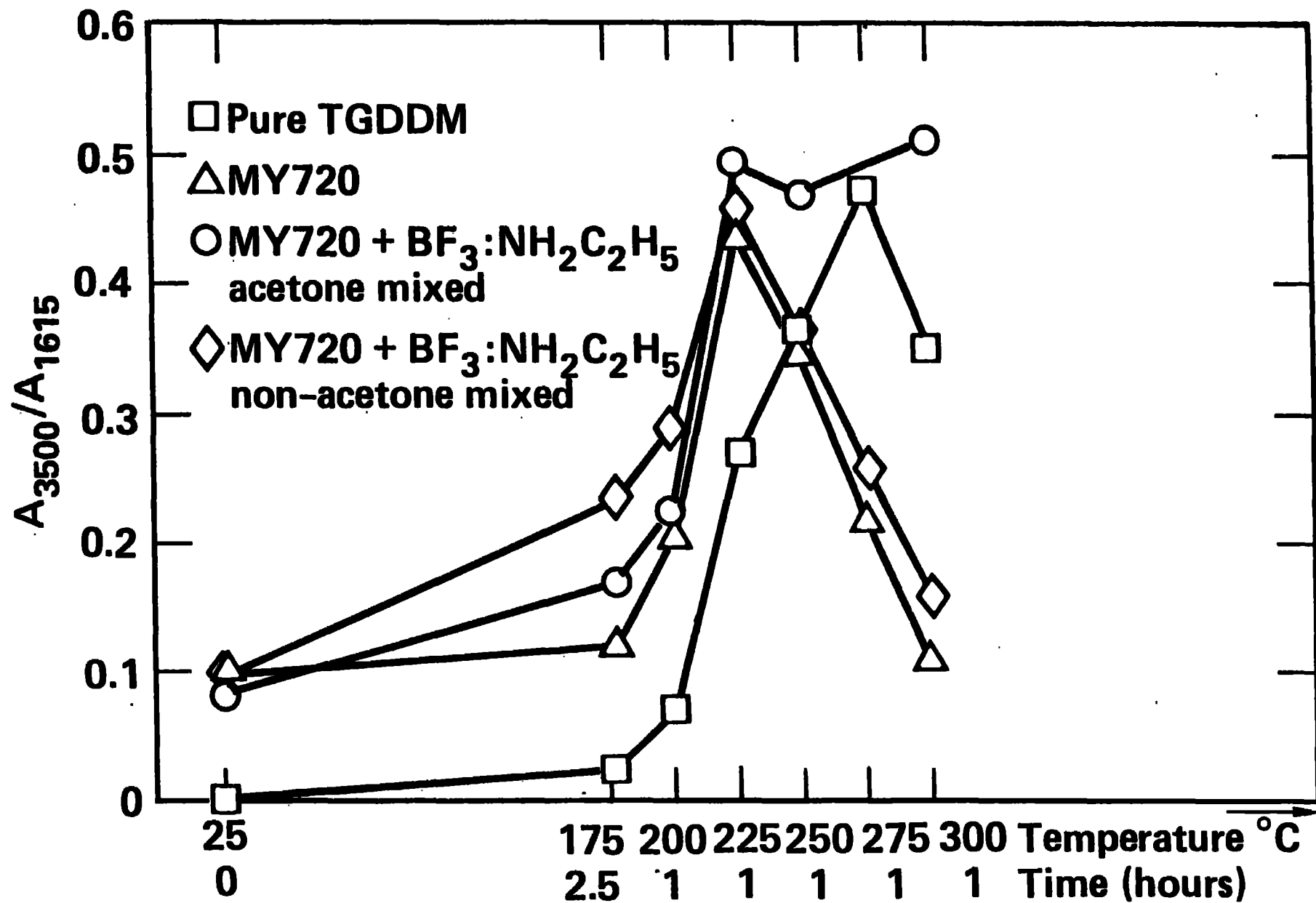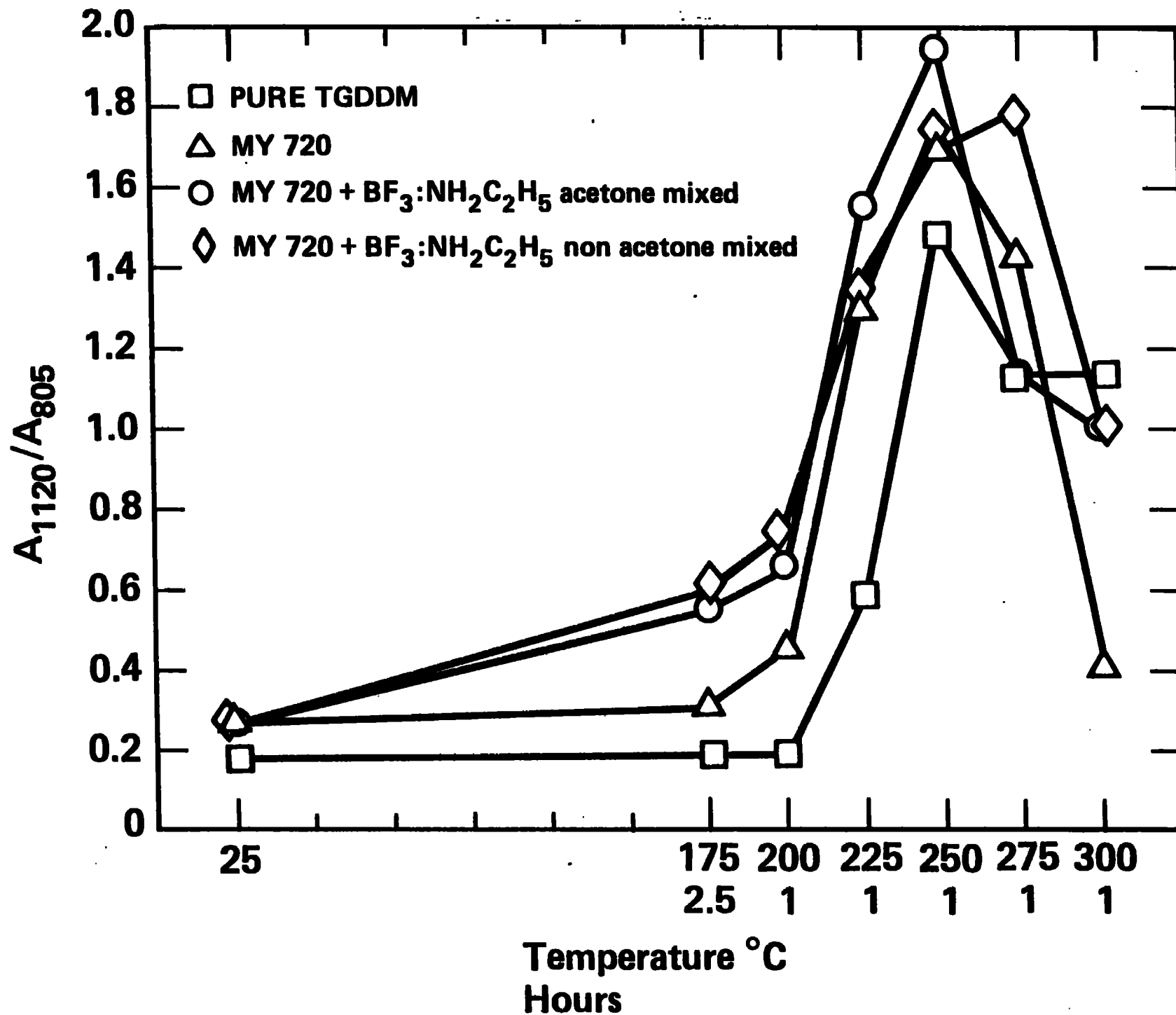
FIGURE 10

FIGURE 11

FIGURE 12
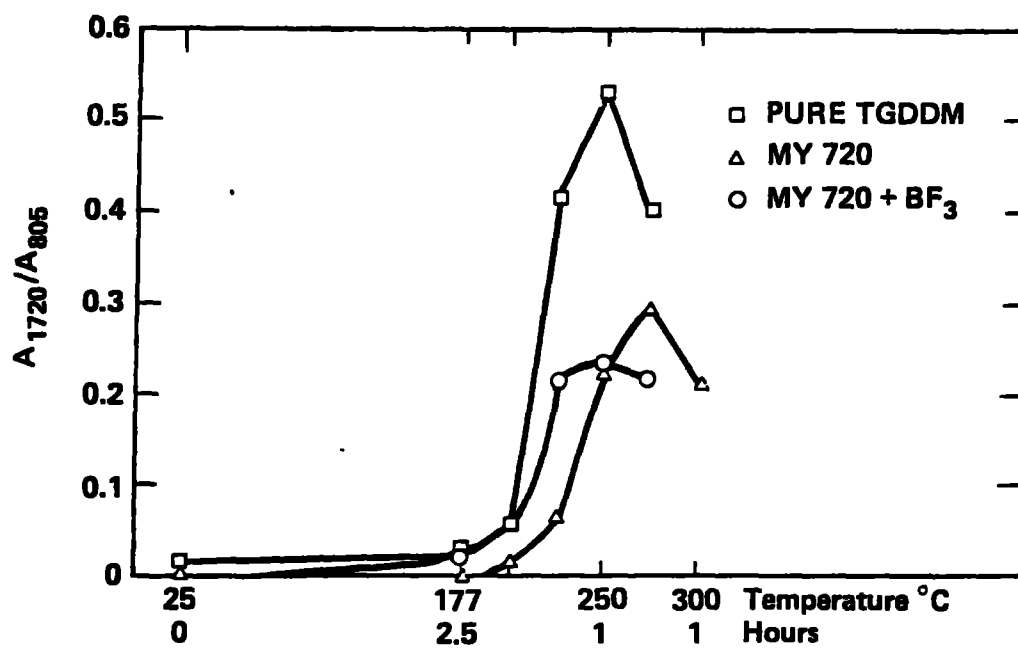
FIGURE 13
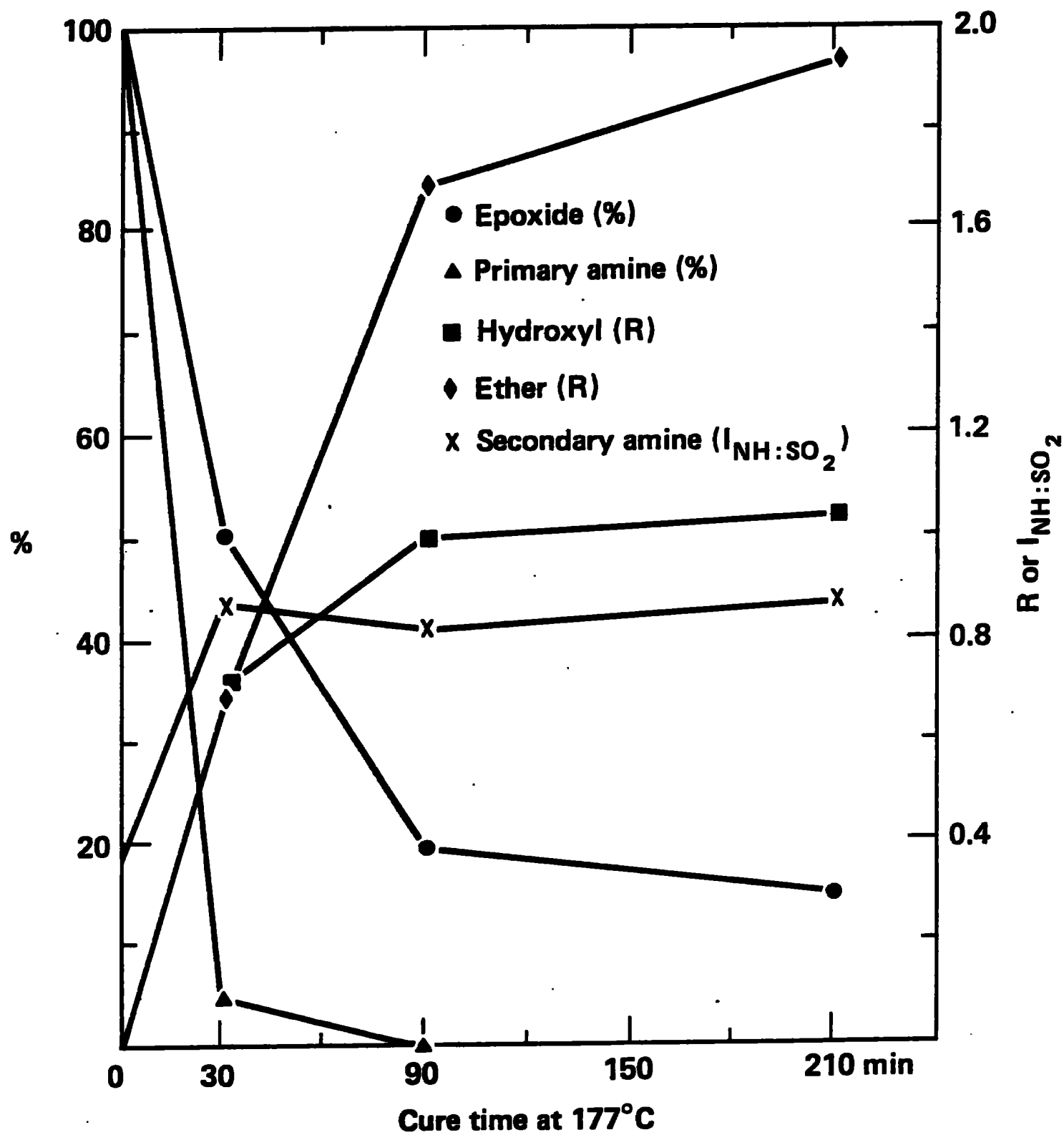
FIGURE 14
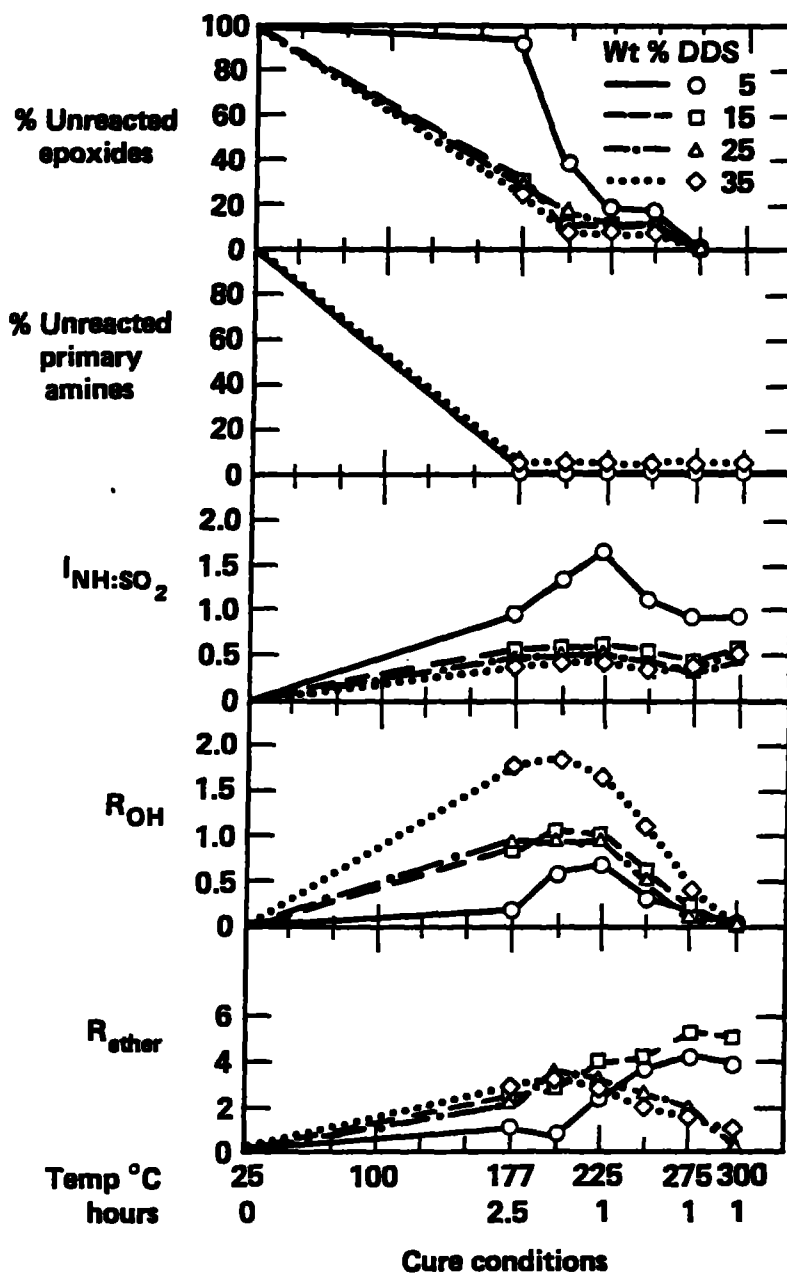
FIGURE 15
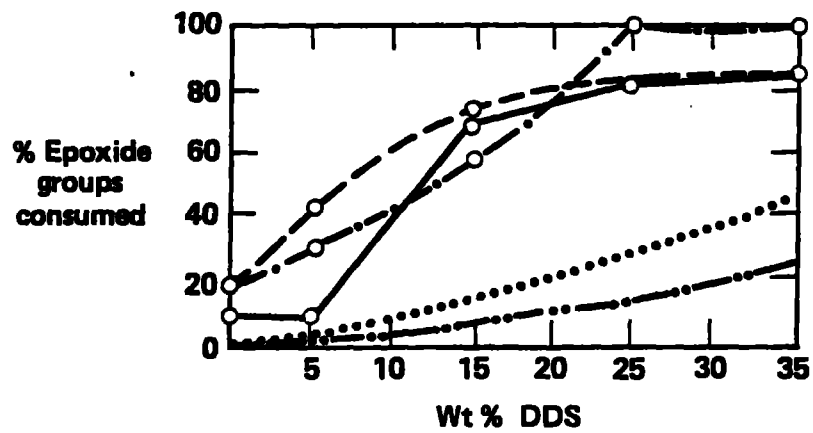
FIGURE 16
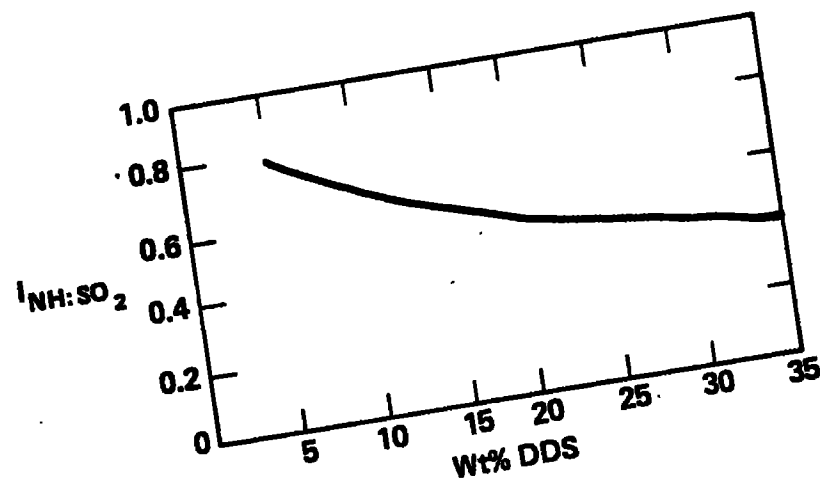
FIGURE 17
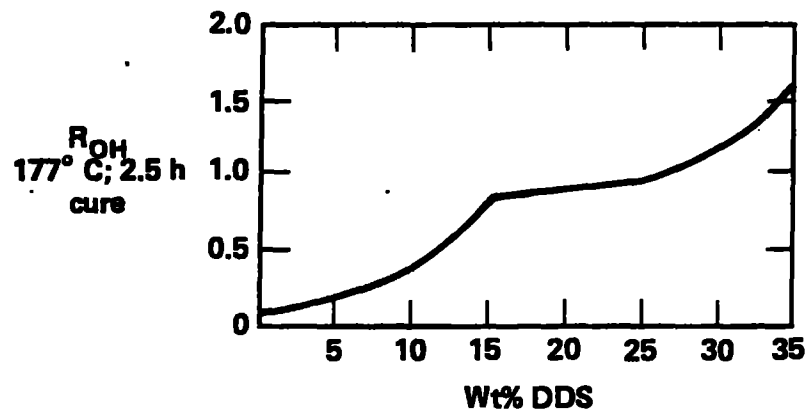
FIGURE 18
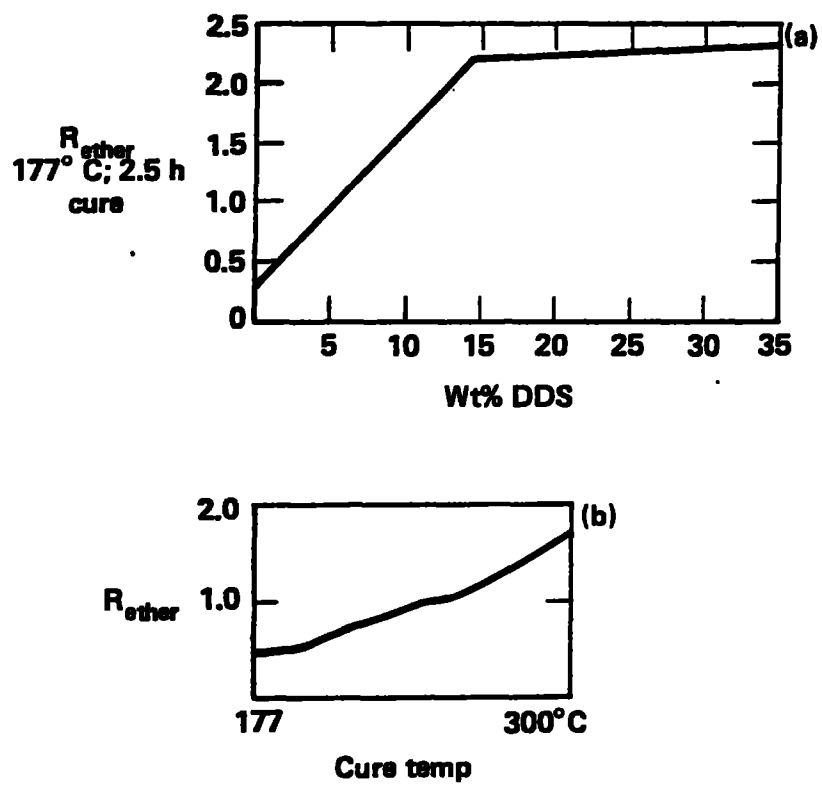
FIGURE 19

% OF EPOXIDES CONSUMED BY EACH CURE REACTION

Total % epoxide consumed ⟶
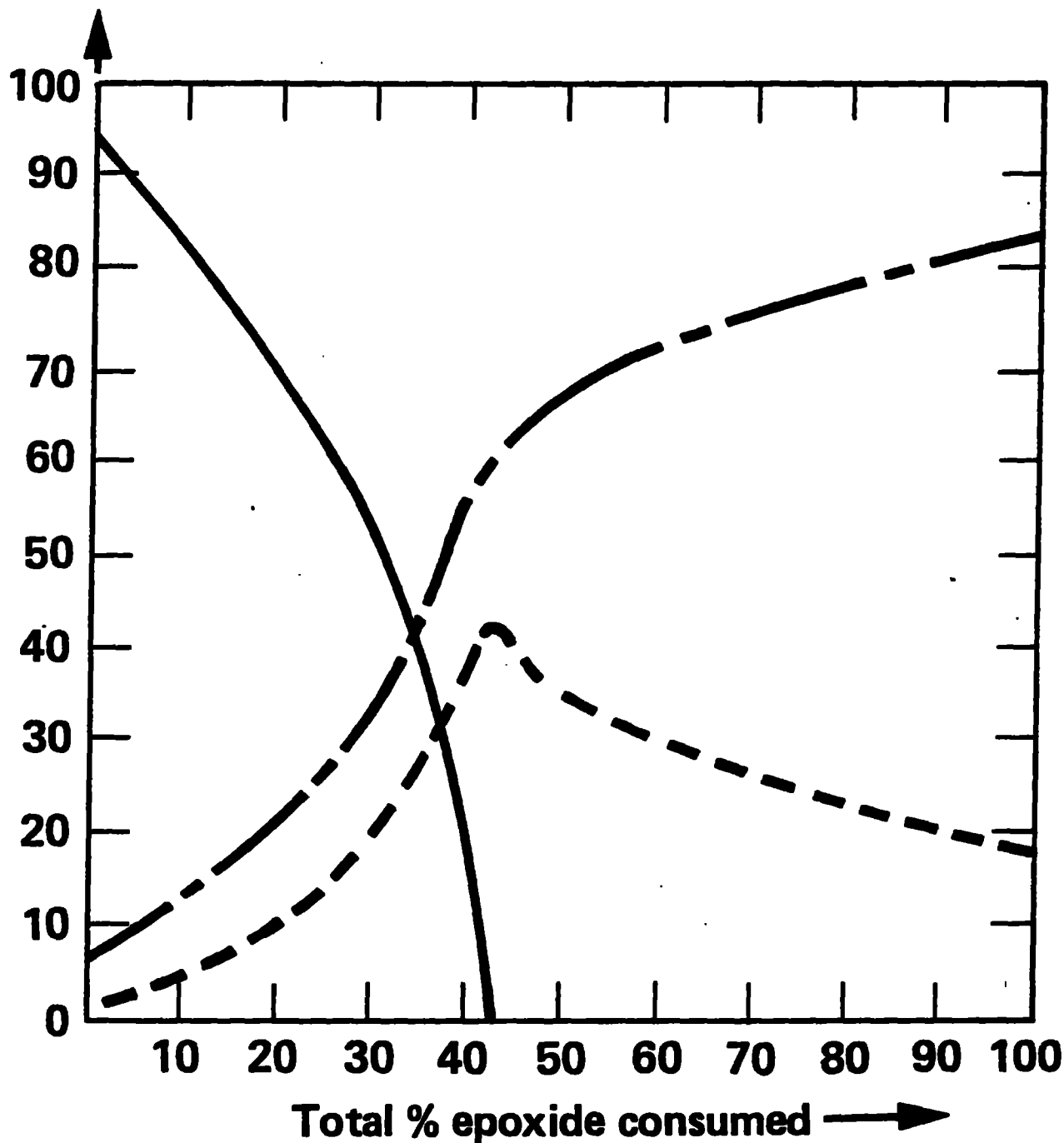
——————— Primary amine–epoxide (PA–E)

— · · — Epoxide–hydroxyl (E–OH)

— — — — Secondary amine–epoxide (SA–E)

FIGURE 20

PRIMARY AMINE-EPOXIDE
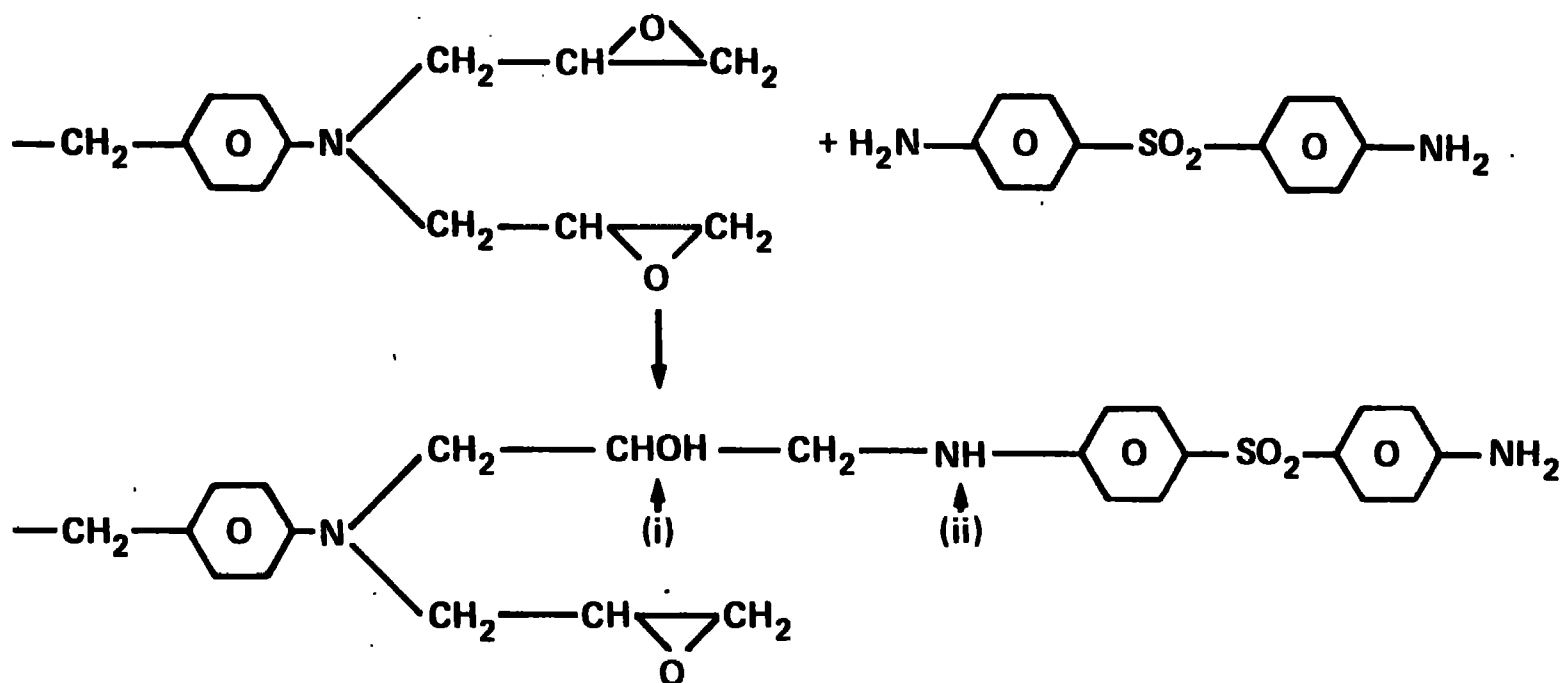
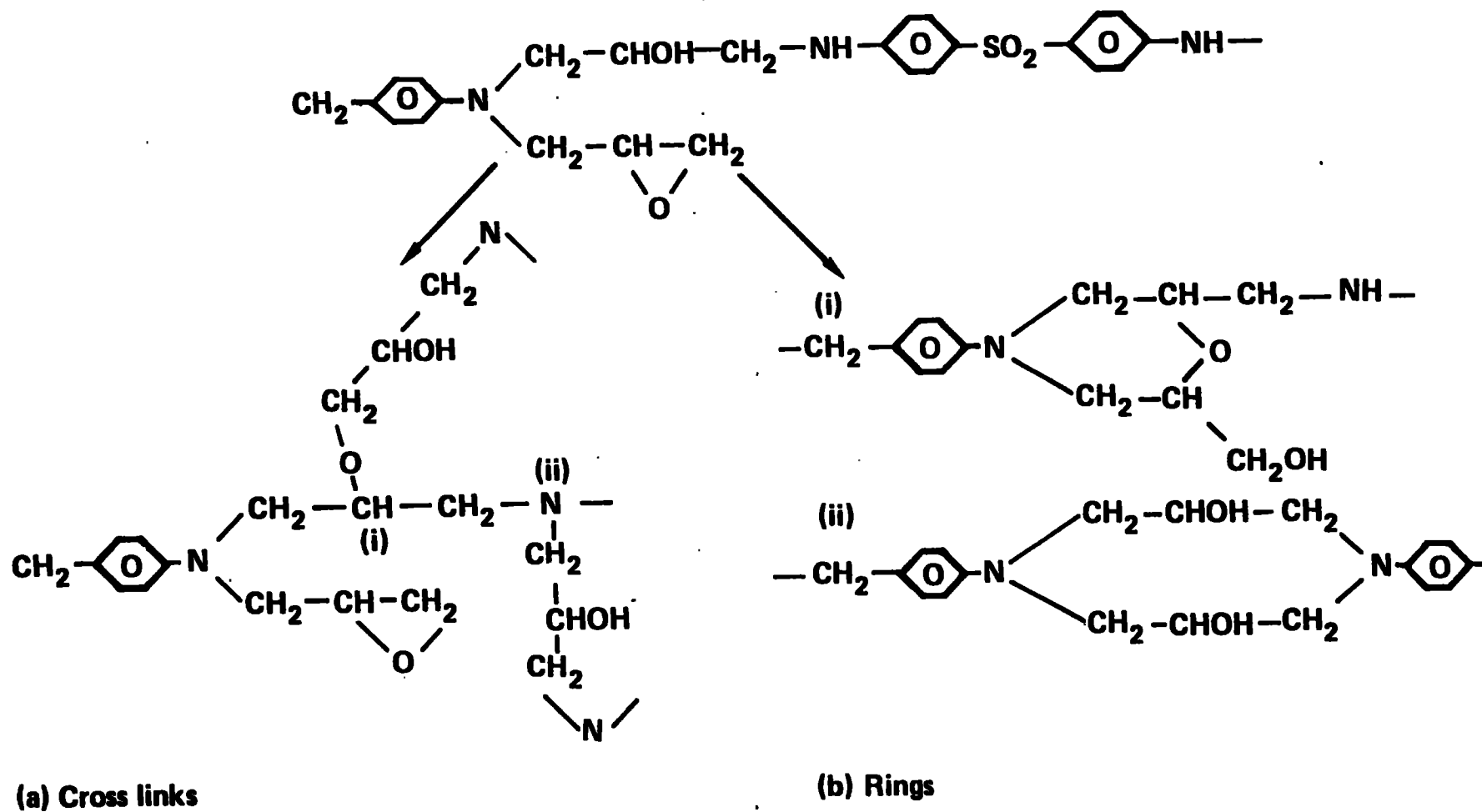
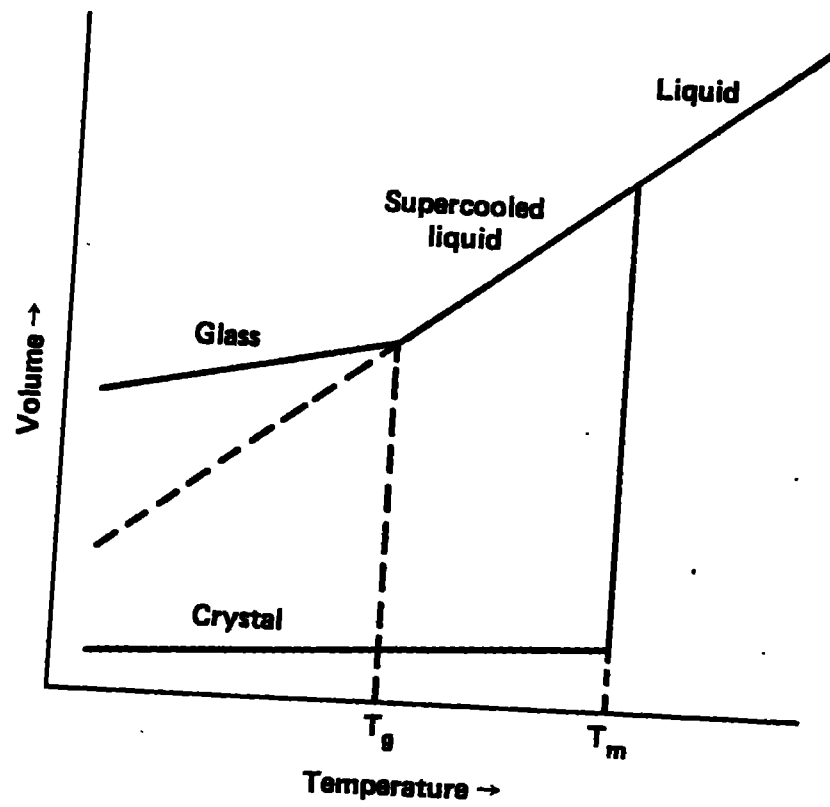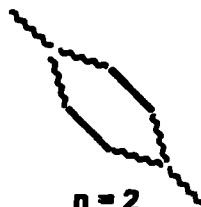FIGURE 21

SECONDARY AMINE-EPOXIDE AND EPOXIDE-HYDROXYL

(a) Cross links

(b) Rings

FIGURE 22

FIGURE 23

Series (A) Sides of rings consist of (1 DGEBA segment + 2 arms of the T403 molecule)n
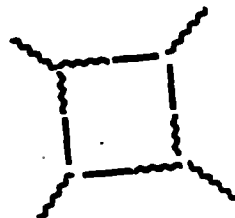
Where n = 1, 2, 3, . . .

n = 1   n = 2

Series (B) Sides of rings consist of (2 DGEBA segments + 2 arms of T403 molecule)n
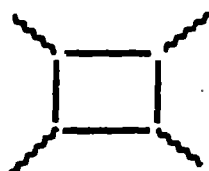
Where n = 1, 2, 3, . . .

n = 1   n = 2

Series (C) Sides of rings consist of (2 DGEBA segments + n DGEBA segments)

Where n = 1, 2, 3, . . .

n = 1   n = 2

T403

DGEBA

FIGURE 24

T403

DGEBA ———

FIGURE 25

	①	②	③	④
Failure stage:	Coarse craze growth prior to crack growth	Slow crack growth through craze midrib	Slow crack growth with small plastic zone at crack tip	Fast unstable crack growth
Craze/crack structure				
Stress at craze/crack surface	*	*		

Distance from tip

| **Resultant fracture topography:** | ———— | Rough initiation region | Smooth mirror region | Rough parabola region |

FIGURE 26

Strain: (%): 0 2·1 3·7 5·3 6·8 8·2 10·1 12·2 15·4 Fractured

Homogeneous
plastic and
elastic
deformation

Onset
inhomogeneous
plastic
deformation

Shear banding
and
necking occurs

FIGURE 27

FIGURE 28